ChemPubSoc Europe

DOI: 10.1002/chem.201405478

CHEMISTRY
A European Journal
Full Paper

Donor–Acceptor Systems

A Series of π-Extended Thiadiazoles Fused with Electron-Donating Heteroaromatic Moieties: Synthesis, Properties, and Polymorphic Crystals

Shin-ichiro Kato,[a] Takayuki Furuya,[a] Masashi Nitani,[b] Naoya Hasebe,[a] Yutaka Ie,[b] Yoshio Aso,[b] Toshitada Yoshihara,[a] Seiji Tobita,[a] and Yosuke Nakamura*[a]

Abstract: π-Extended thiadiazoles **4**–**8** fused with various electron-donating heteroaromatic moieties have been designed and synthesized. Just like thiadiazoles **1**–**3** synthesized previously, **4**–**8** exhibit intramolecular charge-transfer (CT) interactions, moderate-to-good fluorescence quantum yields of up to 0.78, and electrochemical amphoterism. In comparison with **1**–**3**, the benzannulation in thiadiazoles **4**–**7** moderately extends the π conjugation and significantly increases the stability of the cationic species formed upon electrochemical oxidation. The fluorescence quantum yields increase remarkably from **3** to **6** and **7** due to the efficient suppression of nonradiative intersystem crossing resulting from the benzannulation. The properties of **4**–**8** strongly reflect the different species annulated to the pyrrole rings, namely benzothiophene, naphthalene, and benzofuran. Eleven crystals, including poly- and pseudopolymorphic crystals of **1** (**1-Crys.**(**Y**) and **1-Crys.**(**G**)), **2** (**2-Crys.**(**O**) and **2-Crys.**(**G**)), **4** (**4-Crys.**(**O**) and **4-Crys.**(**G**)), and **6** (**6-Crys.**(**O**) and **6-Crys.**(**G**)), were obtained and characterized by X-ray crystallography. The fluorescence colors and efficiencies are distinct for each poly- and pseudopolymorph of **1**, **2**, **4**, and **6**. It has been suggested that both the extent of the electronic interactions in the π-stacked dimers and the presence of excitonic interactions originating in the 1D face-to-face slipped columns affect the fluorescence wavelengths of the poly- and pseudopolymorphs.

Introduction

Flat and rigid π-conjugated organic molecules are endowed with characteristic electronic, photophysical, and electrochemical properties by virtue of the delocalized electrons and thereby are key components in organic and molecular electronics.[1] Research into functional organic materials is constantly evolving in order to fine-tune the electronic structures of π-conjugated molecules and control their solid-state structures to obtain proper intermolecular interactions. In particular, the latter issue is of importance because the electronic properties of π-conjugated molecules in the bulk state significantly depend on their molecular-packing patterns. Along these lines, π-conjugated molecules with fully ring-fused polycyclic skeletons, such as polycyclic aromatic hydrocarbons (PAHs),[2,3] heteroacenes,[4] and ladder compounds with annulated π-conjugated frameworks,[5] are of special interest because their rigid co-planar structures promise enhanced π-conjugation and allow the formation of dense molecular packing in the solid state, leading to intriguing properties such as strong fluorescence and high carrier mobility.

Polarized π-conjugated chromophores consisting of strong electron donors (D) and acceptors (A) connected by a π spacer and thus featuring intramolecular charge-transfer (CT) interactions are promising materials for diverse optoelectronic applications.[6,7] Recently, the intermolecular interactions in these D–A-substituted compounds have attracted attention as a valid force for inducing the growth of well-ordered organic nano- and microstructures. For example, Zhang and co-workers elegantly prepared single-crystal microtubes with rectangular cross-sections from a D–A chromophore containing dicyanovinyl and *N*,*N*-dimethylanilino groups.[8] Liu and co-workers also synthesized various D–A chromophores and demonstrated that they formed hierarchically self-assembled structures.[9] On the other hand, we envisioned that the fusion of electron-donating and -accepting heteroaromatics in ring-fused polycyclic skeletons leads not only to the intramolecular CT interactions characteristic of D–A-substituted compounds but also to efficient intermolecular π–π stacking interactions in the solid state. On this basis we recently designed and synthesized six-ring fused thiadiazoles **1**–**3**[10] in which highly electron-donating thienopyrrole or indole moieties are annulated to an electron-accepting benzothiadiazole (BTD) unit to form a new

[a] *Dr. S.-i. Kato, T. Furuya, N. Hasebe, Dr. T. Yoshihara, Prof. S. Tobita, Prof. Y. Nakamura*
Division of Molecular Science
Faculty of Science and Technology, Gunma University
1-5-1 Tenjin-cho, Kiryu, Gunma 376-8515 (Japan)
E-mail: nakamura@gunma-u.ac.jp

[b] *Dr. M. Nitani, Prof. Y. Ie, Prof. Y. Aso*
The Institute of Scientific and Industrial Research (ISIR)
Osaka University
8-1 Mihogaoka, Ibaraki, Osaka 567-0047 (Japan)

Supporting information for this article is available on the WWW under http://dx.doi.org/10.1002/chem.201405478.

class of D–A-fused chromophores.[11–16] We demonstrated that thiadiazoles **1**–**3** display fluorescence solvatochromism and electrochemical amphoterism as well as forming dense π-stacking structures. These results motivated us to synthesize new thiadiazole congeners with further extended π systems through benzannulation, which was expected to not only enrich the structural scope of thiadiazole π systems, but also create novel properties.

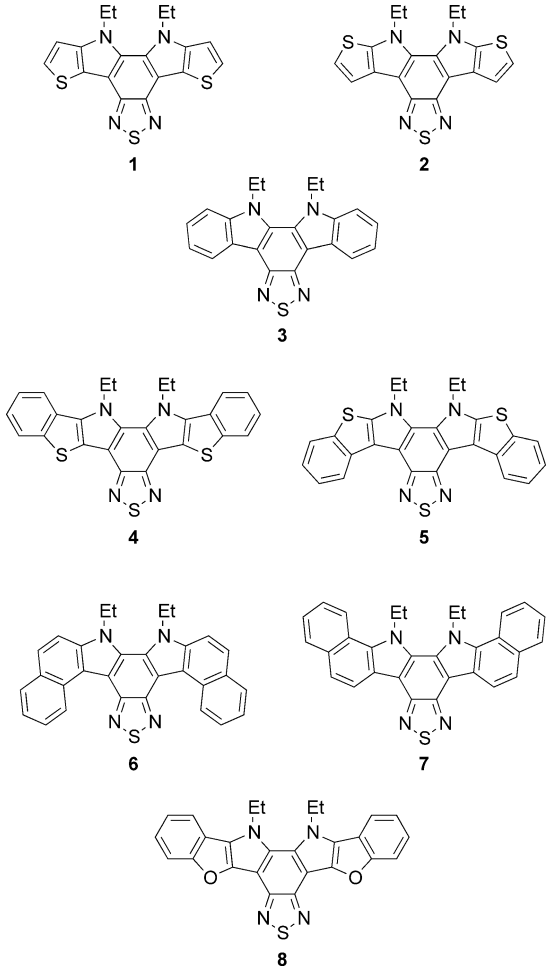

In this study we have designed and synthesized eight-ring fused thiadiazoles **4**–**7**, which are dibenzo-annulated analogues of **1**–**3**, and **8**, in which the sulfur atoms in **4** are replaced by oxygen atoms.[17] By comparing the properties of **1**–**8**, we elucidated the structure–property relationships in π-extended thiadiazoles fused with electron-donating heteroaromatic moieties. During the course of this study we found that the compounds presented herein, with the exception of **5**, afford single crystals that exhibit remarkable fluorescence, and that **1**, **2**, **4**, and **6** form poly- and pseudopolymorphic crystals that show distinct photophysical properties depending on the molecular arrangement. We report herein in detail the synthesis, structural features, and electronic, photophysical, and electrochemical properties of **1**–**8** in solution, as well as their solid-state photophysical properties.

Results and Discussion

Synthesis

The strategy used for the synthesis of **4**–**8** is outlined in Scheme 1. Just like thiadiazoles **1**–**3**, compounds **4**–**8** were synthesized from the known benzothiadiazole derivative **9**[18] in three steps. We first subjected **9** to Migita–Kosugi–Stille coupling reactions with tributyl(aryl)tin derivatives to prepare **10**–**14** in yields of 73–89%. The double-reductive cyclization of **10**–**14** with PPh_3 in *o*-dichlorobenzene (*o*-DCB) was carried out to give the corresponding **15**–**19** in yields of 60–87%.[19] It is worth noting that **18** was obtained as the sole product by using **13** as precursor. The observed regioselectivity of cyclization reflects the higher electron density of the carbon atom at the 1-position of naphthalene compared with at the 2-position. Compounds **4**–**8** were finally obtained by the reaction of **15**–**19** with iodoethane in the presence of NaH as a base in THF. The low yield of **5** is ascribed to the poor solubility of the monoethylated intermediate, some of which precipitated as an orange solid during the reaction at reflux in THF. Unfortunately, in our hands, we were unable to obtain tributyl(3-benzo[*b*]furyl)tin (see Scheme S1 in the Supporting Information),[20] which is a key reagent in the synthesis of the isomer of **8**. All the compounds were fully characterized by various spectroscopic methods. Although the solubility of **5** is poor, compounds **4**, **6**, **7**, and **8** are reasonably soluble in common organic solvents such as toluene, CH_2Cl_2, $CHCl_3$, and acetone.

Photophysical properties in solution

The absorption and fluorescence spectra of **4**–**8** were recorded in various solvents to investigate their photophysical properties in detail, and the relevant data for discussion are summarized in Table 1. We recently found that the longest absorption maxima (λ_{max}^{abs}) and the fluorescence maxima (λ_{max}^{fl}) are increasingly redshifted from **3** to **2** to **1**, and not only the nature of the aromatic rings fused with the pyrrole rings, but also their orientation affect the photophysical properties.[10] Therefore the photophysical data for **4**–**8** are chiefly discussed from the viewpoint of the effects of 1) the extension of multifused π-frameworks compared with **1**–**3**, that is, benzannulation, 2) the nature of the aromatic rings annulated to the pyrrole rings, that is, benzothiophene, naphthalene, and benzofuran, and 3) their orientation.

UV/Vis spectra

The electronic absorption spectra of **1**, **2**, **4**, **5**, and **8** and of **3**, **6**, and **7** in CH_2Cl_2 are shown in Figure 1a and b, respectively. Similarly to **1**–**3**, compounds **4**–**8** feature broad, intramolecular CT bands with the longest λ_{max}^{abs} between 429 and 452 nm. The longest λ_{max}^{abs} values for **4** and **5** are redshifted relative to those for **1** and **2**, respectively (436 (**1**), 425 (**2**), 443 (**4**), and 450 nm (**5**)), which has been attributed to the extension of the π conjugation resulting from the extension of the multifused π frameworks. Likewise, the longest λ_{max}^{abs} values for **6** and **7** are

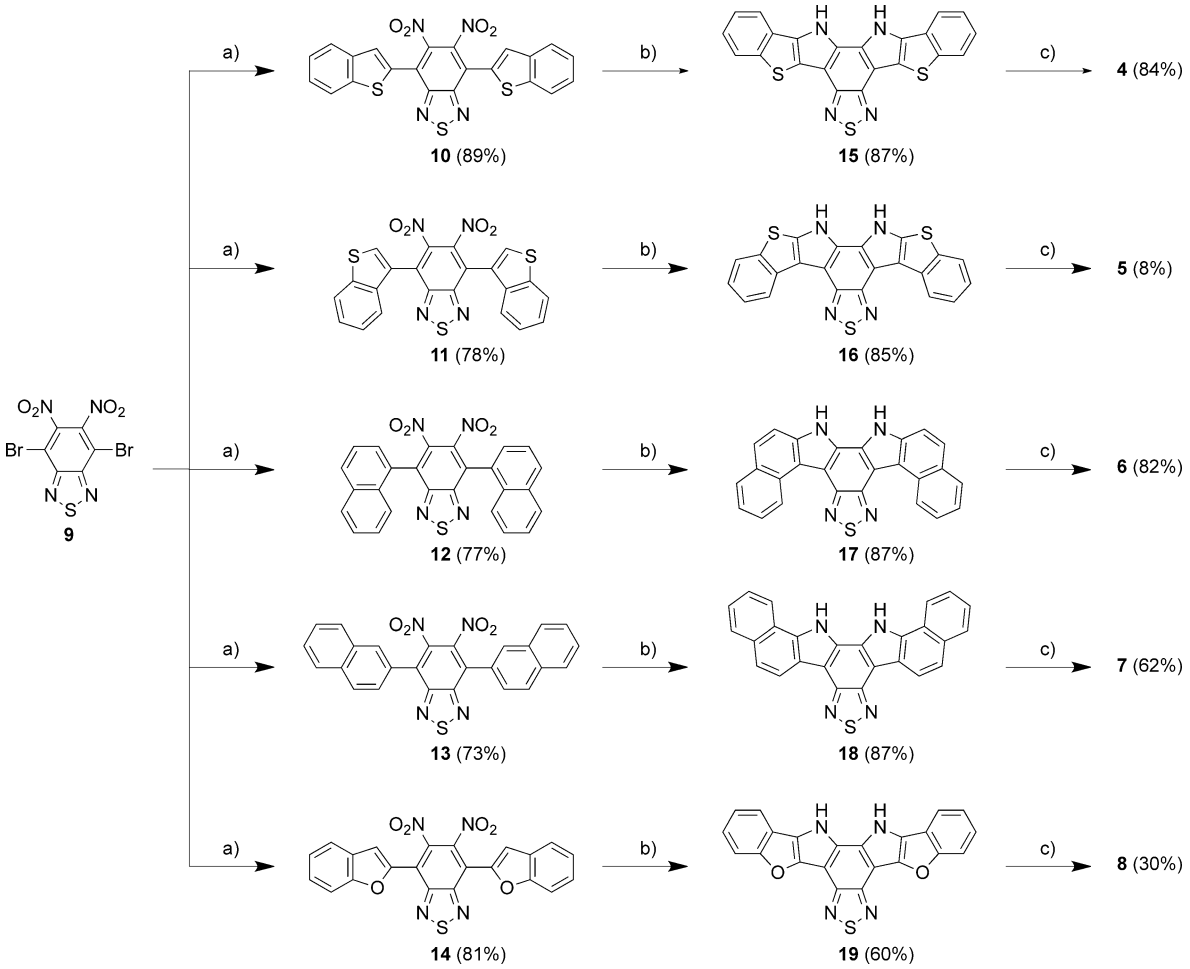

Scheme 1. Synthesis of π-extended thiadiazoles **4**–**8** fused with electron-donating heteroaromatic moieties. Reagents and conditions: a) $[Pd(PPh_3)_4]$, tributyl(2-benzo[*b*]thienyl)tin for **10**, tributyl(3-benzo[*b*]thienyl)tin for **11**, tributyl(1-naphthyl)tin for **12**, tributyl(2-naphthyl)tin for **13**, tributyl(2-benzo[*b*]furyl)tin for **14**, THF or methoxycyclopentane, reflux; b) PPh_3, *o*-dichlorobenzene (*o*-DCB), 180 °C; c) iodoethane, NaH, THF, reflux.

Table 1. Photophysical data for **1**–**8** in solution.[a]

	Solv.	λ_{max}^{abs} [nm (eV)][b]	λ_{max}^{fl} [nm]	τ_f [ns][c]	Φ_f[d]	k_r [10^7 s^{-1}][e]	k_{nr} [10^7 s^{-1}][f]
1	toluene	432 (2.88)	523	19.4	0.73	3.8	1.3
	CH_2Cl_2	436 (2.85)	565	16.6	0.33	2.0	4.0
2	toluene	423 (2.94)	508	13.0	0.45	3.5	4.2
	CH_2Cl_2	425 (2.92)	565	16.6	0.33	2.0	4.0
3	toluene	420[g] (2.96)	470	0.97	0.07	6.9	96
	CH_2Cl_2	420[g] (2.96)	497	1.00	0.04	4.3	95
4	toluene	440 (2.81)	522	10.8	0.78	7.2	2.0
	CH_2Cl_2	443 (2.80)	565	16.3	0.47	2.9	3.3
5	toluene	447 (2.77)	535	15.0	0.56	3.7	2.9
	CH_2Cl_2	450 (2.75)	575	16.1	0.26	1.6	4.6
6	toluene	435 (2.85)	498	5.16	0.42	8.1	11
	CH_2Cl_2	434 (2.86)	526	9.17	0.11	1.2	9.7
7	toluene	428 (2.90)	493	3.91	0.37	9.5	16
	CH_2Cl_2	429 (2.89)	525	8.09	0.21	2.6	9.8
8	toluene	447 (2.77)	535	10.9	0.72	6.6	2.6
	CH_2Cl_2	452 (2.75)	582	14.8	0.41	2.8	4.0

[a] Complete data for **1**–**8** are included in the Supporting Information. [b] Only the longest absorption maxima are shown. [c] Fluorescence lifetime. [d] Absolute fluorescence quantum yields were determined by using an integrating sphere system. [e] Radiative decay constant. [f] Nonradiative decay constant. [g] Shoulder.

redshifted compared with that for **3** (420 nm (**3**), 434 nm (**6**), 429 nm (**7**)). Compounds **4** and **5** or **6** and **7** differ in not only their longest λ_{max}^{abs} values, but also in the shape of the absorption spectra, which suggests that their electronic structures are substantially dependent upon the orientation of the annulated moieties with respect to the pyrrole rings. The longest λ_{max}^{abs} value for **8** is redshifted compared with that for **4** by 9 nm, and hence the trend of increasing λ_{max}^{abs} values in the order naphthalene < benzothiophene < benzofuran holds for **4**–**8**.

DFT calculations

To obtain further insight into the electronic properties, we conducted density functional theory calculations on **4**–**8** as well as on **1**–**3** by using the Gaussian 09 suit of programs.[21] The frontier molecular orbital (FMO) plots were obtained by performing single-point calculations at the B3LYP/6-311G**//B3LYP/6-31G* level of theory (Figure 2). The HOMOs of **4**–**8** are almost delocalized over the whole of the π system except for the sulfur atom in the thiadiazole moiety, just like those of **1**–**3** (see Figure S20 in the Supporting Information), and thus the peripheral benzene rings in **4**–**8** contribute significantly to the HOMOs.

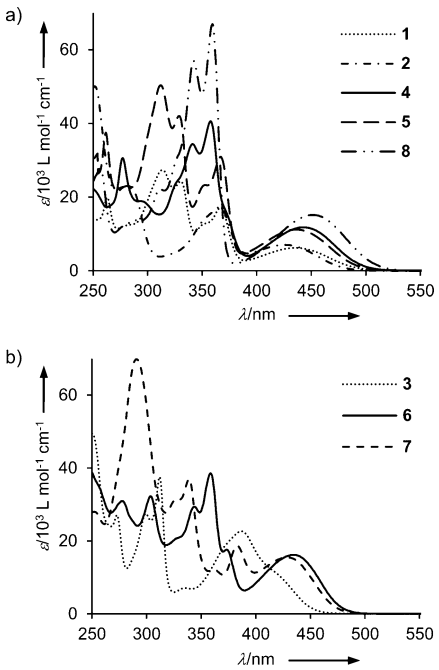

Figure 1. UV/Vis absorption spectra of a) **1**, **2**, **4**, **5**, and **8** and b) **3**, **6**, and **7** in CH_2Cl_2 at room temperature. The data for **5** are plotted with arbitrary intensity due to its low solubility.

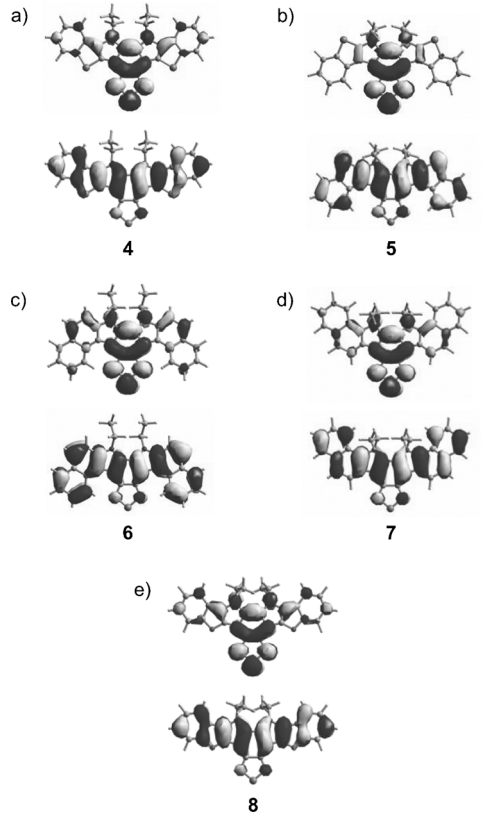

Figure 2. Molecular orbital plots (B3LYP/6-311G**//B3LYP/6-31G*) for a) **4**, b) **5**, c) **6**, d) **7**, and e) **8**. The lower plots represent the HOMOs, the upper plots represent the LUMOs.

This finding again indicates the effective extension of the π conjugation in **4**–**8** compared with in **1**–**3** by benzannulation. In all cases, the LUMOs are mainly localized on the electron-accepting BTD moieties, and hence the peripheral benzene rings make only marginal contributions to the LUMOs of **4**–**8**. Intriguingly, the electron density distribution in the HOMOs of compounds **4** and **5** or **6** and **7** differ depending on the orientation of the annulated moieties with respect to the pyrrole rings, which leads to the differences in their photophysical and electrochemical properties (see below).[22]

We performed time-dependent (TD) DFT calculations on **1**–**8** at the TD-B3LYP/6-31G*//B3LYP/6-31G* level of theory to elucidate their optical absorption properties (see Tables S6–S10 in the Supporting Information). The absorption maxima in the low-energy region of **4**–**8** can be predominantly attributed to the HOMO–LUMO transitions as is the case with **1**–**3**. The important findings in relation to the calculated λ_{max}^{abs} values, which are generally consistent with the absorption spectra, can be summarized as follows. 1) Extension of the multifused π systems leads to redshifted absorptions except in the cases of **1** and **4** (458 nm (**1**), 454 nm (**4**)). 2) The difference in the orientation of the annulated moieties with respect to the pyrrole rings in **4** and **5** or **6** and **7** causes distinct differences in the calculated longest λ_{max}^{abs} (454 nm (**4**), 484 nm (**5**), 466 nm (**6**), 444 nm (**7**)). 3) The replacement of sulfur atoms by oxygen atoms in the electron-donating heteroaromatic moieties results in a moderate redshift of the calculated longest λ_{max}^{abs} (454 nm (**4**), 466 nm (**8**)).

Fluorescence spectra

Figure 3 shows the fluorescence spectra of **1**–**8** in CH_2Cl_2. Similarly to the change in the longest λ_{max}^{abs} values for **1**–**8** described above, the λ_{max}^{fl} values are generally redshifted by benzannulation. Thus, **5**–**7** display redshifted λ_{max}^{fl} values relative to the corresponding **2** and **3** by about 20–30 nm, although **1** and **4** accidentally show identical values of λ_{max}^{fl} of 565 nm. Moreover, as is the case with the longest λ_{max}^{abs} values, the λ_{max}^{fl} values for **4**–**8** are redshifted by changing the moieties annulated to the pyrrole rings from naphthalene, benzothiophene, to benzofuran: The λ_{max}^{fl} values for **4**, **6**, and **8** in CH_2Cl_2 are 565, 526, and 582 nm. Consequently, compound **8** has the longest observed λ_{max}^{fl} among all the compounds in this study.

Notably, pronounced positive fluorescence solvatochromism is observed for **4**–**8**, whereas the absorption spectra of **4**–**8** show only slight changes between those recorded in nonpolar toluene and polar DMF (Table 1).[23] The solvent-dependent spectral changes observed for **4**–**8** are essentially identical to those observed for **1**–**3** previously. Figure 4 shows the fluorescence spectra of **4** in different solvents. The λ_{max}^{fl} values are remarkably redshifted upon increasing the solvent polarity from toluene to DMF (522 nm in toluene, 570 nm in DMF), and the color of the fluorescence changes from green to yellow (see Figure S9 in the Supporting Information). This clearly indicates that **4**–**8** have a more polar electronic structure in the excited state, namely an intramolecular CT state, than in the ground state.

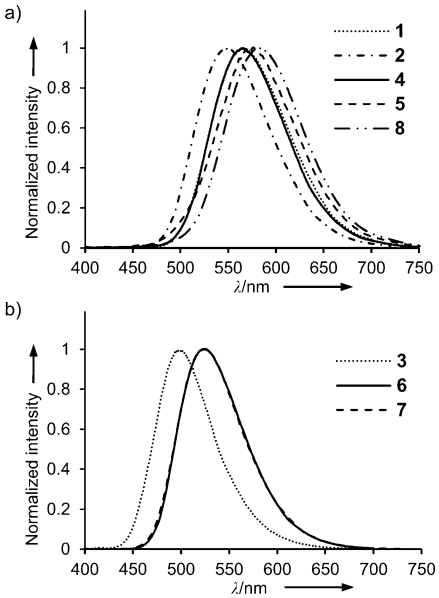

Figure 3. Fluorescence spectra of a) **1**, **2**, **4**, **5**, and **8** (λ_{ex} = 370, 380, 390, 400, and 400 nm, respectively) and b) **3**, **6**, and **7** (λ_{ex} = 370, 390, and 400 nm, respectively) in CH_2Cl_2 at room temperature. The spectra of **6** and **7** accidentally overlap.

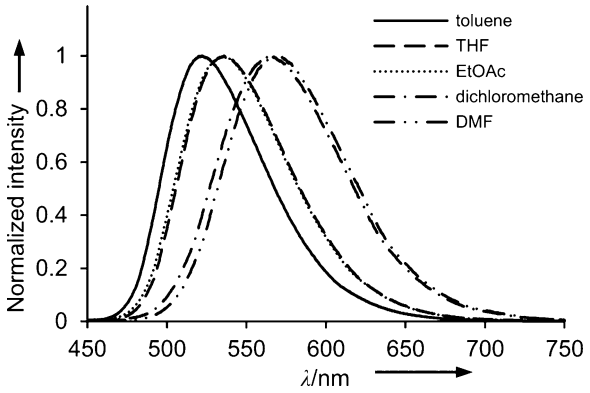

Figure 4. Fluorescence spectra of **4** in different solvents upon excitation at 390 nm at room temperature.

The absolute fluorescence quantum yields (Φ_f) for **1**–**8** in various solvents were determined by using an integrating sphere system (Table 1). We could not find any general relationship between the solvent polarity and the Φ_f values for **1**–**8**. The Φ_f values in CH_2Cl_2 for most compounds seem to be lower than those in other solvents, although the reason for this is unclear at present. We recently demonstrated that the moieties annulated to the pyrrole rings significantly affect the fluorescence efficiency.[10] Compounds **1** and **2** display moderate-to-high Φ_f values of 0.33–0.73 and 0.34–0.51, respectively, whereas **3** displays significantly low Φ_f values of 0.04–0.07. The quantum yields (Φ_{isc}) for intersystem crossing in **1**, **2**, and **3** in toluene are 0.26, 0.56, and 0.94, respectively. Thus, the extremely fast intersystem crossing to the triplet state in **3** compared with in **1** and **2** is responsible for the low Φ_f values for **3**. The extension of the multifused π frameworks from **1** and **2** to **4** and **5** results in marginal changes in the Φ_f values; **4** and **5** exhibit Φ_f values of 0.47–0.78 and 0.26–0.63, respectively (see Table S2 in the Supporting Information for the complete data). Unexpectedly, **6** and **7** display very high Φ_f values (0.11–0.43 for **6** and 0.21–0.42 for **7**) compared with **3**. Nevertheless, the annulation of benzothiophene moieties to the pyrrole rings is likely to yield higher Φ_f values than the annulation of naphthalene moieties. Comparing **4** and **8**, the replacement of sulfur atoms by oxygen atoms has almost no effect on the fluorescence efficiency; the Φ_f values for **8** (0.34–0.72) are comparable to those of **4**.

To obtain further insight into the photophysical properties of **1**–**8**, we determined their fluorescence lifetimes (τ_f) by using the time-correlated single-photon counting method and calculated the radiative (k_r) and nonradiative (k_{nr}) decay rate constants from the singlet excited state according to $k_r = \Phi_f/\tau_f$ and $k_{nr} = (1-\Phi_f)/\tau_f$ (Table 1). No pronounced differences in the τ_f values are observable upon extension of the multifused π frameworks from **1** and **2** to **4** and **5**, respectively; the τ_f values for **4** (10.8–16.6 ns) are slightly shorter than those for **1** (16.6–24.2 ns) , and the τ_f values for **5** (15.0–17.0 ns) are similar to those for **2** (13.0–16.8 ns). The values of both k_r and k_{nr} for **4** are larger than those for **1**, whereas the values of k_r and k_{nr} for **5** are comparable to those for **2**. The τ_f, k_r, and k_{nr} values for **8** are similar to those for **4**, which demonstrates that the replacement of sulfur atoms by oxygen atoms in the electron-donating heteroaromatic moieties barely affects the radiative and nonradiative processes. Notably, **6** and **7** show very high τ_f values compared with **3** (0.97–1.07 ns (**3**), 5.16–9.29 ns (**6**), 3.91–8.09 ns (**7**)). The calculated k_{nr} values for **6** and **7** ($(6.1–15)\times10^7\ s^{-}$) are significantly smaller than those for **3** ($(89–96)\times10^7\ s^{-}$), whereas the k_r values for **6** and **7** are comparable to those for **3**. Time-resolved photoacoustic measurements gave Φ_{isc} values in toluene of 0.61 and 0.67 for **6** and **7**, respectively, which are almost two-thirds the value for **3** (see Figures S10–S12 in the Supporting Information).[24] In **6** and **7**, as is the case with **3**, the sum of Φ_f and Φ_{isc} is almost equal to 1, within experimental error, which clearly indicates on the basis of the equation $\Phi_f + \Phi_{isc} + \Phi_{ic} = 1$, in which Φ_{ic} is the quantum yield of internal conversion, that internal conversion in **6** and **7** barely occurs. From these results it can be concluded that higher values of Φ_f for **6** and **7** than for **3** derive from the effective suppression of intersystem crossing by benzannulation.

Electrochemical properties

We performed cyclic voltammetry (CV) experiments on **1**–**8** in *o*-DCB (0.1 mol L^{-1} *n*$BuNPF_6$, standard Fc^+/Fc) to investigate their electrochemical properties (Table 2).[25] As described above, we recently found that **1**–**3** display amphoteric electrochemical behavior due to the presence of the electron-withdrawing BTD moiety and the electron-donating thienopyrrole or indole moieties. Compounds **1**–**3** have similar acceptor abilities; they exhibit almost the same reduction onsets (E^{red}_{onset}). On the other hand, they differ in their donor ability, with **1** and **2** showing oxidation onsets (E^{ox}_{onset}) cathodically shifted relative

Table 2. Oxidation and reduction potentials of **1**–**8** determined by CV in *o*-DCB (0.1 mol L^{-1} nBuNPF$_6$),[a] theoretically calculated HOMO and LUMO levels,[b] and electrochemical (ΔE_{redox}) and optical energy gaps (ΔE_{opt}).

	E^{ox}_{onset} (E_{pa}) [V]	E^{red}_{onset} (E_{pc}) [V]	HOMO [eV]	LUMO [eV]	ΔE_{redox} [V][c]	ΔE_{opt} [eV][d]
1	+0.31[e] (+0.46)	−2.23[f] (−2.42)	−5.18	−2.00	2.54	2.85
2	+0.40[g] (+0.59) (+1.12)	−2.25[f] (−2.51)	−5.24	−1.91	2.65	2.92
3	+0.62[e] (+0.77)	−2.22[f] (−2.39)	−5.52	−2.13	2.84	2.96
4	+0.35[f] (+0.51) (+1.01)	−2.15[f] (−2.33)	−5.18	−2.00	2.50	2.80
5	+0.27[f] (+0.39) (+0.83)	−2.21[g] (−2.34)	−5.14	−2.07	2.48	2.75
6	+0.40[f] (+0.56) (+1.09)	−2.26[f] (−2.48)	−5.19	−2.07	2.66	2.86
7	+0.50[f] (+0.65) (+1.34)	−2.21[f] (−2.40)	−5.37	−2.12	2.71	2.89
8	+0.27[f] (+0.39) (+0.89)	−2.15[f] (−2.31)	−5.11	−2.03	2.42	2.74

[a] All potentials are given versus the Fc^+/Fc couple used as external standard. Scan rate: 100 mV s^{-1}. [b] Calculated at the B3LYP/6-311G**//B3LYP/6-31G* level of theory. [c] The electrochemical gap, ΔE_{redox}, is defined as the potential difference between E^{ox}_{onset} and E^{red}_{onset}. [d] The optical gap, ΔE_{opt}, is defined as the energy corresponding to the λ^{abs}_{max} in CH_2Cl_2. [e] Irreversible wave. [g] Quasireversible wave. [f] Reversible wave.

to **3**, which apparently reflects the difference in the electron-donating ability of thiophene and benzene. As expected, **4**–**8** also show amphoteric electrochemical behavior within the available potential window (Figure 5).

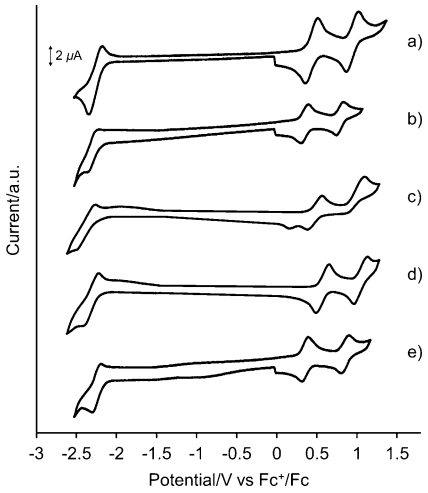

Figure 5. Cyclic voltammograms of a) **4**, b) **5**, c) **6**, d) **7**, and e) **8** measured in *o*-DCB (0.1 mol L^{-1} nBuNPF$_6$) at a scan rate of 100 mV s^{-1}.

No pronounced difference in the E^{red}_{onset} values (−2.26 to −2.15 V) was observed for **1**–**8**, but their E^{ox}_{onset} values turned out to be significantly dependent on the structure. Although the E^{ox}_{onset} value for **4** is only slightly more anodic than that for **1** (+0.31 V (**1**), +0.35 V (**4**)), the E^{ox}_{onset} value for **5** is more cathodic than that for **2** (+0.40 V (**2**), +0.27 V (**5**)), and the values for **6** and **7** are also more cathodic than that for **3** (+0.62 V (**3**), +0.40 V (**6**), +0.50 V (**7**)). This finding indicates that the benzannulation essentially enhances the donor ability. From **6** and **7**, **4** and **5**, to **8**, the oxidations occur cathodically, which reflects the differences in the electron-donating ability of naphthalene, benzothiophene, and benzofuran; the HOMO levels of these moieties were calculated to be −6.04, −6.10, and −6.23 eV, respectively, at the B3LYP/6-311G**//B3LYP/6-31G* level of theory.[26] In the series **4**–**8**, the trend in the electrochemical HOMO–LUMO gaps (ΔE_{redox}) almost corresponds to that of the E^{ox}_{onset} values, and a good correlation exists between the ΔE_{redox} values and the optical HOMO–LUMO gaps (ΔE_{opt}).

Compounds **1**–**8** show quasireversible or reversible reduction waves, and although the first oxidation waves for **1**–**3** are quasireversible or irreversible, those for **4**–**8** are reversible. Moreover, in contrast to **1** and **3**, which show a large peak amplitude after the first oxidation, reversible second oxidation waves are observable for **4**, **5**, **7**, and **8**. These results demonstrate that the benzannulation effectively enhances the stability of the cationic species formed upon electrochemical oxidation.

Photoluminescent colors of the crystals

Organic molecules that exhibit solid-state emissions have attracted considerable attention not only in the fundamental research of their photophysical properties, but also in materials science.[27] It is well known that most organic fluorophores are almost nonluminescent or only faintly emissive in the solid state, even if they are highly emissive in solution, owing to the concentration quenching caused by intermolecular interactions.[27a,28] We obtained 11 single crystals of **1**–**4** and **6**–**8** (see Figure S5 in the Supporting Information),[29] including poly- and pseudopolymorphic crystals of **1** (**1-Crys.**(**Y**) and **1-Crys.**(**G**)), **2** (**2-Crys.**(**O**) and **2-Crys.**(**G**)), **4** (**4-Crys.**(**O**) and **4-Crys.**(**G**)), and **6** (**6-Crys.**(**O**) and **6-Crys.**(**G**)), suitable for X-ray crystallographic analysis, and found that most of them show remarkable fluorescence (Figures 6 and S6). It is considered that in the thiadiazole derivatives presented herein, the energy transfer in the excited state is substantially inhibited owing to large Stokes shifts, that is, the small overlap between the UV/Vis and fluorescence spectra, which leads to the observed solid-state fluorescence.

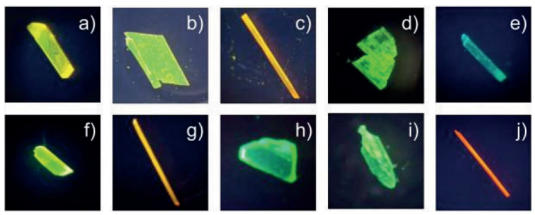

Figure 6. Photographs of a) **1-Crys.**(**Y**), b) **1-Crys.**(**G**), c) **2-Crys.**(**O**), d) **2-Crys.**(**G**), e) **3-Crys.**, f) **4-Crys.**(**G**), g) **6-Crys.**(**O**), h) **6-Crys.**(**G**), i) **7-Crys.**, and j) **8-Crys.** under UV irradiation (365 nm).

X-ray crystal structures

We recently reported that the crystallization of **1** and **2** by vapor diffusion of hexane into CH_2Cl_2 solutions of the mole-

cules afforded the crystals **1-Crys.**(**Y**) and **2-Crys.**(**G**), respectively (Figure 6 a,d);[10] the crystals **1-Crys.**(**G**) and **2-Crys.**(**O**) (Figure 6b,c) were obtained as minor products under the same crystallization conditions, that is, **1-Crys.**(**Y**) and **1-Crys.**(**G**) or **2-Crys.**(**G**) and **2-Crys.**(**O**) were obtained concomitantly. Likewise, vapor diffusion of hexane into a CH_2Cl_2 solution of **6** gave **6-Crys.**(**G**) as the major product along with **6-Crys.**(**O**) as the minor product (Figure 6g,h). We could not find the crystallization conditions for the selective formation of specific polymorphs of **1**, **2**, and **6**, even after repeated trials. However, we were able to isolate the different polymorphs by hand by using a microscope because of their different colors and shapes (see Figure S5 in the Supporting Information), which allowed the polymorphs to be characterized individually. The selective formation of two polymorphs of **4** was achieved by changing the solvent of recrystallization. Thus, pseudopolymorphs **4-Crys.**(**O**) and **4-Crys.**(**G**) were obtained by vapor diffusion of hexane into CH_2Cl_2 and toluene solutions of **4**, respectively; toluene molecules are included in a 4:1 stoichiometry in **4-Crys.**(**G**).[30]

π-Stacked dimer structures

In **1-Crys.**(**Y**), **2-Crys.**(**O**), **2-Crys.**(**G**), **4-Crys.**(**O**), **4-Crys.**(**G**), **6-Crys.**(**O**), and **6-Crys.**(**G**) as well as in the crystal of **8** (abbreviated as **8-Crys.**),[31] two neighboring molecules form π-stacked dimer structures in a head-to-tail arrangement to cancel the dipole (Figures 7 and S4 in the Supporting Information). In the dimers, the molecules are arranged longitudinally in a slipped π-stacked fashion at a distance of 3.34–3.76 Å. In contrast, in **1-Crys.**(**G**) as well as in the crystal of **3** (abbreviated as **3-Crys.**), two neighboring molecules are mutually almost orthogonal, with the molecules lying in parallel with a combination of π–π and CH–π interactions between the ethyl groups and the π planes. In the π-stacked dimer structures described above, the electron-donating moieties, namely thienopyrrole, indole, benzothienopyrrole, benzindole, or benzofuropyrrole, overlap with the electron-withdrawing BTD moieties, which suggests the presence of intermolecular CT interactions; no π-stacked dimer structure was observed in the crystal of **7** (abbreviated as **7-Crys.**). The polymorphs **1-Crys.**(**Y**) and **1-Crys.**(**G**), **2-Crys.**(**O**) and **2-Crys.**(**G**), and **6-Crys.**(**O**) and **6-Crys.**(**G**) differ in the extent of overlap and/or the distance between the two π planes in their π-stacked dimers, whereas the dimer structure of pseudopolymorph **4-Crys.**(**O**) is almost identical to that of **4-Crys.**(**G**). The X-ray structures of the poly- and pseudopolymorphs of **1**, **2**, **4**, and **6** are discussed further below, mainly from the viewpoint of their molecular arrangements.

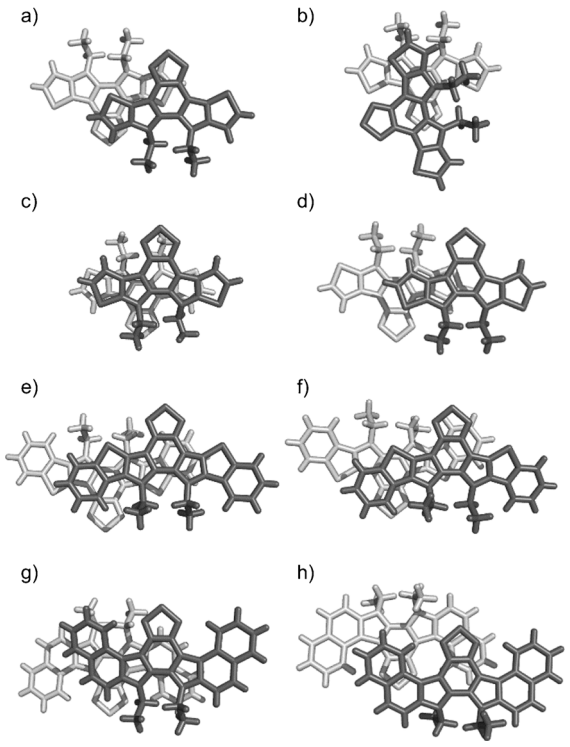

Figure 7. Arrangement of neighboring molecules in the polymorphs of a) **1-Crys.**(**Y**), b) **1-Crys.**(**G**), c) **2-Crys.**(**O**), d) **2-Crys.**(**G**), e) **4-Crys.**(**O**), f) **4-Crys.**(**G**), g) **6-Crys.**(**O**), and h) **6-Crys.**(**G**).

Packing structures

Figure 8 shows the packing diagrams for the crystal structures of **1**, **2**, **4**, and **6**. With the exception of **6-Crys.**(**G**), 1D molecu-

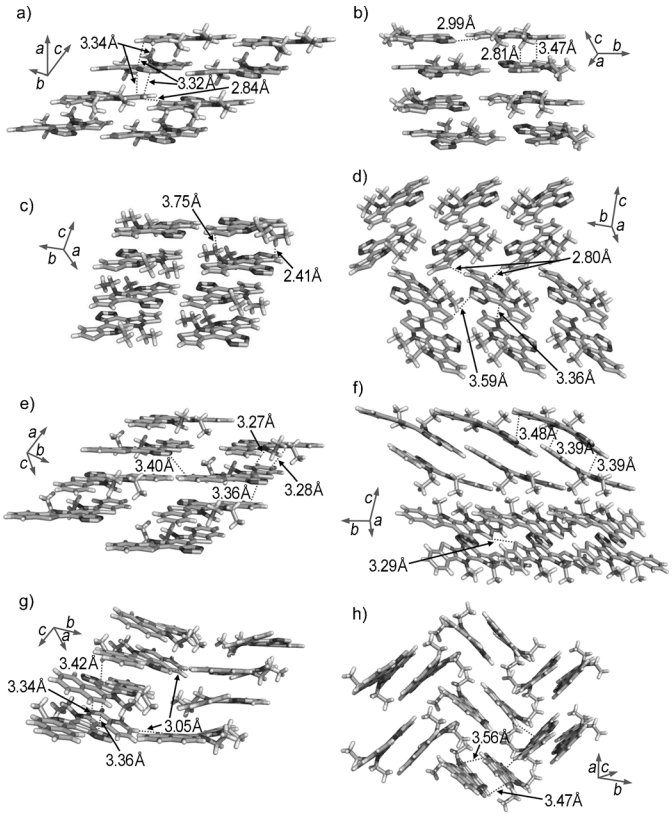

Figure 8. Molecular packing in crystals of a) **1-Crys.**(**Y**), b) **1-Crys.**(**G**), c) **2-Crys.**(**O**), d) **2-Crys.**(**G**), e) **4-Crys.**(**O**), f) **4-Crys.**(**G**), g) **6-Crys.**(**O**), and h) **6-Crys.**(**G**). The solvent molecules in **4-Crys.**(**G**) have been omitted for clarity. The structures of **1-Crys.**(**Y**) and **2-Crys.**(**G**) have been reported previously.[10] The packing structures of **3-Crys.**, **7-Crys.**, and **8-Crys.** are included in the Supporting Information.

lar networks are observed. In **1-Crys.**(**Y**), **2-Crys.**(**O**), **4-Crys.**(**O**), and **6-Crys.**(**O**), the π-stacked dimers interact with other π-stacked dimers through π–π stacking interactions to form 1D face-to-face slipped-column structures (Figure 8a,c,e,g). The angles ($\theta_{\pi\text{-stack}}$) between the π planes and the stacking axes in **1-Crys.**(**Y**), **4-Crys.**(**O**), and **6-Crys.**(**O**) are almost identical, whereas that in **2-Crys.**(**O**) is significantly larger ($\theta_{\pi\text{-stack}} = 31^\circ$ for **1-Crys.**(**Y**), 69° for **2-Crys.**(**O**), 32° for **4-Crys.**(**O**), and 36° for **6-Crys.**(**O**)). The columns in **1-Crys.**(**Y**) and **6-Crys.**(**O**) assemble through weak S–H (2.84 Å for **1-Crys.**(**Y**) and 3.05 Å for **6-Crys.**(**O**)) interactions, whereas the columns in **4-Crys.**(**O**) assemble through S–π (3.40 Å) interactions. In **2-Crys.**(**O**), no favorable interaction between neighboring columns is observed.

The packing motifs of **1-Crys.**(**G**), **2-Crys.**(**G**), **4-Crys.**(**G**), and **6-Crys.**(**G**) are apparently different to those of the corresponding **1-Crys.**(**Y**), **2-Crys.**(**O**), **4-Crys.**(**O**), and **6-Crys.**(**O**). In **1-Crys.**(**G**), the dimers of **1** form cross-stacked columns along the *c* axis, and the columns assemble through weak S–H (2.99 Å) interactions (Figure 8b). The dimers in **2-Crys.**(**G**) are packed in a sandwich-herringbone motif with a 1D array along the *b* axis as a result of S–S (3.59 Å) and CH–π interactions (Figure 8d). The dimers in **4-Crys.**(**G**) provide 1D brick-like columns along the *b* axis through π–π stacking (3.39 and 3.48 Å) and S–S (3.29 Å) interactions (Figure 8f).[32] In **6-Crys.**(**G**), the dimers interact with other dimers through CH–π interactions, and typical edge-to-face herringbone structures are formed (Figure 8h). The packing motifs of the polymorphs of **1**, **2**, and **6** may reflect the structural features of the π-stacked dimers, such as the orientation, the extent of overlap, and the distance between conjugated π planes.[33] The significant differences in the packing structures of **4-Crys.**(**O**) and **4-Crys.**(**G**) can be attributed to the fact that molecules of toluene from the recrystallization solvent are included in **4-Crys.**(**G**).[34]

The π-stacked dimers in **3-Crys.** form a cross-stacked column structure as is the case with **2-Crys.**(**G**) (see Figure S1a in the Supporting Information). On the other hand, the dimers in **8-Crys.** form a 1D face-to-face slipped column structure (see Figure S1d) as observed in **1-Crys.**(**Y**), **4-Crys.**(**O**), and **6-Crys.**(**O**).

Solid-state photophysical properties

We recorded the fluorescence emission and excitation spectra of crystalline samples of **1**–**4** and **6**–**8** to investigate their solid-state photophysical properties (Figure 9 and Table 3).[35,36] The emission maxima ($\lambda_{max}^{fl(solid)}$) of the crystals are redshifted by 13–80 nm relative to the corresponding emission maxima ($\lambda_{max}^{fl(tol)}$) in toluene, in which the contribution from solvent stabilization should be less than that from other solvents. The largest difference between the $\lambda_{max}^{fl(solid)}$ and $\lambda_{max}^{fl(tol)}$ values is found in **6-Crys.**(**O**) ($\lambda_{max}^{fl(solid)} = 578$ nm, $\lambda_{max}^{fl(tol)} = 498$ nm); the fluorescence colors of **6-Crys.**(**O**) and a toluene solution of **6** are orange and green, respectively (Figure 6g). Accordingly, the $\lambda_{max}^{fl(solid)}$ value for **6-Crys.**(**O**) is redshifted compared with those for **4-Crys.**(**O**) and **4-Crys.**(**G**), although **4** shows a redshifted fluorescence maximum relative to **6** in toluene. Of the crystals described here, **8-Crys.** exhibits the most redshifted $\lambda_{max}^{fl(solid)}$ value of 608 nm (Figure 6j). The fluorescence quantum yields (Φ_f^{solid}) in the solid state are lower than those in toluene solution. It would appear that the substantial redshifts of $\lambda_{max}^{fl(solid)}$ and the lower values of Φ_f^{solid} observed in the solid-state fluorescence

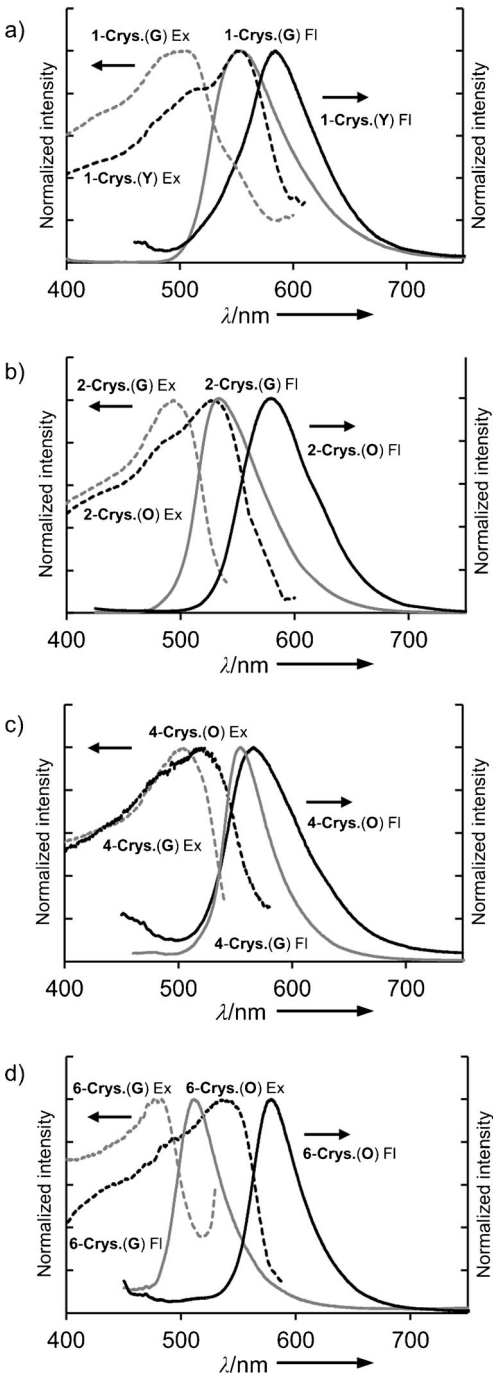

Figure 9. Fluorescence excitation (Ex: dashed lines) and emission (Fl: solid lines) spectra of the poly- and pseudopolymorphs: a) **1-Crys.**(**Y**) and **1-Crys.**(**G**), b) **2-Crys.**(**O**) and **2-Crys.**(**G**), c) **4-Crys.**(**O**) and **4-Crys.**(**G**), and d) **6-Crys.**(**O**) and **6-Crys.**(**G**). An excitation wavelength of 390 nm was used for **1-Crys.**(**Y**), **1-Crys.**(**G**), **2-Crys.**(**O**), and **2-Crys.**(**G**), and of 400 nm for **4-Crys.**(**O**), **4-Crys.**(**G**), **6-Crys.**(**O**), and **6-Crys.**(**G**). The fluorescence excitation spectra of **1-Crys.**(**Y**), **1-Crys.**(**G**), **2-Crys.**(**O**), **2-Crys.**(**G**), **4-Crys.**(**O**), **4-Crys.**(**G**), **6-Crys.**(**O**), and **6-Crys.**(**G**) were monitored at 630, 620, 580, 580, 600, 580, 610, and 520 nm, respectively.

Table 3. Photophysical data for the crystalline samples of **1**–**4** and **6**–**8**.[a]

	$\lambda_{max}^{fl(solid)}$ [nm]	λ_{max}^{ex} [nm]	Φ_f^{solid}[b]
1-Crys.(**Y**)	584	551	0.14
1-Crys.(**G**)	557	500[c]	0.10
2-Crys.(**O**)	580	526	0.19
2-Crys.(**G**)	534	490	0.13
3-Crys.	505	462	0.03
4-Crys.(**O**)	566	517	<0.01
4-Crys.(**G**)[d]	545	500	0.17
6-Crys.(**O**)	578	536	0.25
6-Crys.(**G**)	511	478	0.03
7-Crys.	520	471	0.11
8-Crys.[e]	608	569	0.11

[a] The data for powder samples obtained by grinding the crystals are included in the Supporting Information. [b] The absolute quantum yields were determined by using an integrating sphere system. [c] Shoulder. [d] (**4**)$_4$·toluene. [e] **8**·$(CHCl_3)_2$.

mainly derive from intermolecular π–π-stacking interactions;[37] the reason for the extremely low value of Φ_f^{solid} (<0.01) for **4-Crys.**(**O**) is not clear at present.

Intriguingly, both the $\lambda_{max}^{fl(solid)}$ values and the fluorescence excitation maxima (λ_{max}^{ex}) are different for **1-Crys.**(**Y**) and **1-Crys.**(**G**), **2-Crys.**(**O**) and **2-Crys.**(**G**), **4-Crys.**(**O**) and **4-Crys.**(**G**), and **6-Crys.**(**O**) and **6-Crys.**(**G**), with crystals of **1-Crys.**(**Y**), **2-Crys.**(**O**), **4-Crys.**(**O**), and **6-Crys.**(**O**) exhibiting redshifted fluorescence emission and excitation spectra in comparison with **1-Crys.**(**G**), **2-Crys.**(**G**), **4-Crys.**(**G**), and **6-Crys.**(**G**), respectively, by 17–67 nm (Table 3). This finding clearly indicates that the electronic and photophysical properties of crystals of **1**, **2**, **4**, and **6** depend on the arrangements of the π-conjugated molecules; effects of the toluene molecules in **4-Crys.**(**G**) on the $\lambda_{max}^{fl(solid)}$ and λ_{max}^{ex} values cannot be excluded.[38]

To assess the effects of the electronic structures of the π-stacked dimers, namely the smallest supramolecular units, on the solid-state emission of the poly- and pseudopolymorphs, we conducted single-point calculations (B3LYP/6-311G**) on the isolated monomers and π-stacked dimers of **1**, **2**, **4**, and **6** on the basis of their X-ray crystal structures (see Table S4 in the Supporting Information). The calculated HOMO–LUMO gaps ($\Delta E_{H\text{-}L}$) of the dimers of **1**, **2**, **4**, and **6** are all smaller than those of the corresponding monomers by 0.02–0.25 eV; in general the HOMO levels increase and the LUMO levels decrease from the monomers to the dimers.[39] The difference (0.02 eV) between the $\Delta E_{H\text{-}L}$ values for the monomer and dimer in **6-Crys.**(**G**) is particularly small compared with those for other crystals, which may reflect the relatively small overlap of the π-conjugated planes in the dimer molecules in **6-Crys.**(**G**) (Figure 7h). Notably, the $\Delta E_{H\text{-}L}$ values of the dimers in **1-Crys.**(**Y**), **2-Crys.**(**O**), and **6-Crys.**(**O**) are less than those in **1-Crys.**(**G**), **2-Crys.**(**G**), and **6-Crys.**(**G**), respectively, by 0.14–0.23 eV, whereas the $\Delta E_{H\text{-}L}$ value of the dimer in **4-Crys.**(**O**) is comparable to that in **4-Crys.**(**G**). These results suggest that the electronic coupling interactions in the dimers in **1-Crys.**(**Y**), **2-Crys.**(**O**), and **6-Crys.**(**O**) are stronger than those in **1-Crys.**(**G**), **2-Crys.**(**G**), and **6-Crys.**(**G**), respectively, which should be responsible for the pronounced redshifts in the $\lambda_{max}^{fl(solid)}$ and λ_{max}^{ex} values of **1-Crys.**(**Y**), **2-Crys.**(**O**), and **6-Crys.**(**O**) relative to those of **1-Crys.**(**G**), **2-Crys.**(**G**), and **6-Crys.**(**G**).[40] The intermolecular distances (*d*) between the center of the BTD moiety and the π plane of the facing molecule in **2-Crys.**(**O**) and **6-Crys.**(**O**) are larger than those in the corresponding **2-Crys.**(**G**) and **6-Crys.**(**G**); the *d* values in **2-Crys.**(**O**), **2-Crys.**(**G**), **6-Crys.**(**O**), and **6-Crys.**(**G**) are 3.76, 3.45, 3.54, and 3.39 Å, respectively. This suggests that the extent of overlap of the π-conjugated planes has a larger effect on the electronic structures of the dimers than the intermolecular distances. Overall, it is considered that the photophysical properties of the crystalline samples mainly reflect the electronic features of the π-stacked dimers determined by a delicate balance of the arrangement (orientation, distance, and extent of overlap) of the π-conjugated planes.

In addition to the electronic coupling of neighboring molecules,[41] the excitonic coupling interactions of the transition dipole moments of the molecules, which extend further than solely the nearest neighbors, affect the solid-state optical and photophysical properties.[42] According to the electron distribution in the HOMOs and LUMOs of **1**–**8** (Figure 2), their transition dipole moments are oriented along the long axis of the molecules (Figure 10). The $\theta_{\pi\text{-stack}}$ values in **1-Crys.**(**Y**), **4-Crys.**(**O**), and **6-Crys.**(**O**) (31, 32, and 36°, respectively) as well as that in **8-Crys.** (37°) are apparently less than the "magic angle" of 54.7° of Kasha's exciton theory.[43] Consequently, it is likely that the packing modes, namely 1D face-to-face slipped column structures, in polymorphs **1-Crys.**(**Y**), **4-Crys.**(**O**), and **6-Crys.**(**O**) as well as **8-Crys.** mainly contain the components of *J*-type aggregates. The unique properties of the *J*-aggregates include redshifted fluorescence and narrowed bandwidths,[44] and thus the redshifted $\lambda_{max}^{fl(solid)}$ values of **1-Crys.**(**Y**), **4-Crys.**(**O**), and **6-Crys.**(**O**) compared with those of **1-Crys.**(**G**), **4-Crys.**(**G**), and **6-Crys.**(**G**), respectively, have in part been attributed to the *J*-aggregate-derived excitonic coupling interactions in the former. Again, the remarkably redshifted $\lambda_{max}^{fl(solid)}$ of **8-Crys.** relative to the $\lambda_{max}^{fl(tol)}$ of **8** by 73 nm is thought to be due to the formation of *J*-aggregates in the crystalline state; however, the $CHCl_3$ molecules included in **8-Crys.** are also likely to affect its $\lambda_{max}^{fl(solid)}$ value.[45] The full widths at half-maximum height (FWHMs) of the emission bands of **6-Crys.**(**O**) and **8-Crys.** are apparently narrower than those of **6** and **8** in toluene, respectively (FWHM = 1470, 1600, 2550, and 2550 cm^{-1} for **6-Crys.**(**O**), **8-Crys.**, **6** in toluene, and **8** in toluene, respectively). On the other hand, the FWHMs of the emission bands of **1-Crys.**(**Y**) and **4-Crys.**(**O**) are almost comparable to those of **1** and **4** in toluene, respectively (FWHM = 2200, 2290, 2610, and

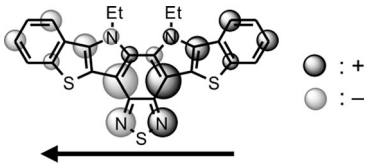

Figure 10. Schematic representation of the transition dipole moment of **4**. The total transition moment is qualitatively shown by the arrow.

2560 cm^{-1} for **1-Crys.**(**Y**), **4-Crys.**(**O**), **1** in toluene, and **4** in toluene, respectively), which implies moderate excitonic interactions in **1-Crys.**(**Y**) and **4-Crys.**(**O**). Although the molecules in **2-Crys.**(**O**) also form 1D face-to-face slipped column structures, the slip angle (69°) in **2-Crys.**(**O**) is larger than those in **1-Crys.**(**Y**), **4-Crys.**(**O**), and **6-Crys.**(**O**), and the extent of overlap of the π planes in **2-Crys.**(**O**) is greater than those in **1-Crys.**(**Y**), **4-Crys.**(**O**), and **6-Crys.**(**O**). This finding implies that **2-Crys.**(**O**) contains many more *H*-type than *J*-type aggregates; however, it is not clear at present why the $\lambda_{max}^{fl(solid)}$ (580 nm) of **2-Crys.**(**O**) is significantly redshifted compared with the $\lambda_{max}^{fl(tol)}$ (508 nm) of **2**.[46]

Conclusion

We have synthesized new π-extended thiadiazoles **4**–**8** fused with electron-donating heteroaromatics by Stille cross-coupling reactions of **9** with the corresponding aryltin derivatives, followed by PPh_3-mediated reductive cyclizations as the key steps. By investigating the electronic, photophysical, and electrochemical properties of **1**–**8** in solution, we have demonstrated the particular importance of benzannulation on their properties. The benzannulation extends the π conjugation and increases the stability of the cationic species formed upon electrochemical oxidation. Moreover, the benzannulation remarkably increases the fluorescence efficiencies of **6** and **7** relative to **3** due to the efficient suppression of nonradiative intersystem crossing in **6** and **7**. We have also shown that the electronic and electrochemical properties of **4**–**8** reflect the differences in the donor potency of the moieties annulated to the pyrrole rings, that is, naphthalene, benzothiophene, and benzofuran.

Eleven crystals were obtained, including the poly- and pseudopolymorphic crystals of **1**, **2**, **4**, and **6**, and the fluorescence colors and efficiencies of **1-Crys.**(**Y**) and **1-Crys.**(**G**), **2-Crys.**(**O**) and **2-Crys.**(**G**), **4-Crys.**(**O**) and **4-Crys.**(**Y**), and **6-Crys.**(**O**) and **6-Crys.**(**G**) were found to be different. The molecular systems reported herein are fairly complicated, and so at present it is not easy to provide quantitative discussions on the correlation between the molecular arrangement and the photophysical properties of the crystals. However, extensive X-ray crystallographic analyses and DFT calculations strongly indicate that the photophysical properties of the poly- and pseudopolymorphs are affected by both the extent of the electronic interactions in the π-stacked dimers and the presence of excitonic interactions originating in the 1D face-to-face slipped columns. We believe that this study will provide not only a useful guideline for tuning the properties of π-extended thiadiazoles but also on their ability to act as fluorophores in the crystalline state. The further derivatization of π-extended thiadiazoles is underway in our laboratory.

Experimental Section

General procedure for the Migita–Kosugi–Stille coupling reactions: Argon was bubbled through a mixture of **9** (1 equiv) and tributyl(aryl)tin (ca. 3.2 equiv) in THF or methoxycyclopentane for 30 min. $[Pd(PPh_3)_4]$ (0.05 equiv) was added to the mixture, and the resulting mixture was heated at reflux. The mixture was cooled to room temperature, and the solvent removed in vacuo. The residue was subjected to column chromatography.

General procedure for PPh_3-mediated reductive cyclization reactions: Argon was bubbled through a mixture of dinitro compounds **10**–**14** (1 equiv) and PPh_3 (10 equiv) in *o*-DCB for 15 min with stirring at 180 °C. The mixture was cooled to room temperature, and the solvent removed in vacuo. The residue was subjected to column chromatography.

General procedure for *N*-ethylation: A mixture of π-extended thiadiazoles **15**–**19** (1 equiv), iodoethane (ca. 6.5 equiv), and sodium hydride (ca. 34 equiv) in THF were heated at reflux in a sealed bottle. The mixture was then poured into water, and the resulting suspension was extracted with $CHCl_3$. The combined organic phases were washed with water, dried over $MgSO_4$, and evaporated in vacuo. The residue was subjected to column chromatography.

Preparation of 10: Compound **9** (150 mg, 0.39 mmol) was allowed to react with tributyl(2-benzo[*b*]thienyl)tin (413 mg, 0.98 mmol) in the presence of $[Pd(PPh_3)_4]$ (22 mg, 0.020 mmol) in THF (15 mL) for 19 h according to the general procedure for Migita–Kosugi–Stille coupling. The crude product was subjected to column chromatography (silica gel, toluene/hexane. 1:1), and the collected material was subsequently washed with hexane to give **10** (171 mg, 0.35 mmol, 89%) as a yellow solid. An analytical sample was obtained by reprecipitation from $CHCl_3$/hexane. M.p. >300 °C; ^1H NMR (600 MHz, $CDCl_3$): $\delta = 7.94$–7.92 (m, 4H), 7.76 (s, 2H), 7.49–7.45 ppm (m, 4H); ^{13}C NMR (150 MHz, $CDCl_3$): $\delta = 152.48$, 139.08, 129.73, 128.49, 126.51, 126.01, 125.31, 125.14, 122.70, 122.34 ppm (one signal is missing); UV/Vis (CH_2Cl_2): λ_{max} (ε) = 293 (24200), 444 nm (9600 $M^{-1}cm^{-1}$); MS (MALDI-TOF, CHCA, positive): *m/z*: 490.57 $[M+H]^+$; elemental analysis calcd (%) for $C_{22}H_{10}N_4O_4S_3$: C 53.87, H 2.05, N 11.42; found: C 53.99, H 2.26, N 11.06.

Preparation of 11: Compound **9** (150 mg, 0.39 mmol) was allowed to react with tributyl(3-benzo[*b*]thienyl)tin (423 mg, 1.00 mmol) in the presence of $[Pd(PPh_3)_4]$ (22 mg, 0.020 mmol) in THF (15 mL) for 19 h according to the general procedure for Migita–Kosugi–Stille coupling. The crude product was subjected to column chromatography (silica gel, toluene/hexane, 2:3), and the collected material was subsequently washed with hexane to give **11** (149 mg, 0.30 mmol, 78%) as orange solids. An analytical sample was obtained by reprecipitation from $CHCl_3$/hexane. M.p. 214–215 °C; ^1H NMR (400 MHz, $CDCl_3$): $\delta = 8.00$ (d, $J = 8.0$ Hz, 2H), 7.82 (d, $J = 6.8$ Hz, 2H), 7.48–7.36 ppm (m, 6H); ^{13}C NMR (150 MHz, $CDCl_3$): $\delta =$ 153.11, 153.04, 143.72, 139.91, 137.63, 137.56, 129.78, 129.61, 125.58, 125.27, 125.19, 125.16, 124.78, 124.69, 123.25, 123.22, 122.56, 122.45 ppm (two pairs of signals are observed due to slow conformational exchange on the NMR timescale); UV/Vis (CH_2Cl_2): λ_{max} (ε) = 259 (21200), 291 (13400), 300 (15100), 431 nm (4000 $M^{-1}cm^{-1}$); MS (MALDI-TOF, CHCA, positive): *m/z*: 490.95 $[M+H]^+$; elemental analysis calcd (%) for $C_{22}H_{10}N_4O_4S_3$: C 53.87, H 2.05, N 11.42; found: C 53.71, H 2.23, N 11.30.

Preparation of 12: Compound **9** (100 mg, 0.26 mmol) was allowed to react with tributyl(1-naphthyl)tin (341 mg, 0.82 mmol) in the presence of $[Pd(PPh_3)_4]$ (16 mg, 0.014 mmol) in methoxycyclopentane (25 mL) for 14 h according to the general procedure for Migita–Kosugi–Stille coupling. The crude product was subjected to column chromatography (silica gel, toluene/hexane, 1:1) and the collected material was subsequently washed with hexane to give **12** (96 mg, 0.20 mmol, 77%) as an orange solid. An analytical sample was obtained by reprecipitation from $CHCl_3$/hexane. M.p. 274–276 °C; ^1H NMR (600 MHz, $[D_6]$DMSO): $\delta = 8.17$ (d, $J = 7.2$ Hz, 2H), 8.09 (d, $J = 7.8$ Hz, 2H), 7.79 (d, $J = 8.4$ Hz, 1H), 7.73–7.69 (m,

4H), 7.64–7.61 (m, 3H), 7.54–7.49 ppm (m, 2H); ^{13}C NMR (150 MHz, [D$_6$]DMSO): δ = 152.56, 152.87, 142.43, 142.33, 132.68, 132.66, 131.04, 130.74, 129.62, 129.02, 128.86, 128.38, 128.28, 128.06, 127.76, 127.45, 126.77, 126.42, 126.32, 125.99, 125.94, 125.25, 125.21, 124.70, 124.68 ppm (two pairs of signals are observed due to slow conformational exchange on the NMR timescale); UV/Vis (CH_2Cl_2): λ_{max} (ε) = 272 (19900), 284 (19200), 406 nm (2200 $M^{-1}cm^{-1}$); MS (MALDI-TOF, Dith, positive): *m/z*: 504.52 [*M*+Na]$^+$; elemental analysis calcd (%) for $C_{26}H_{14}N_4O_4S$·0.01$CHCl_3$: C 65.13, H 2.94, N 11.68; found: C 65.05, H 3.17, N 11.56.

Preparation of 13: Compound **9** (156 mg, 0.41 mmol) was allowed to react with tributyl(2-naphthyl)tin (506 mg, 1.21 mmol) in the presence of [Pd(PPh$_3$)$_4$] (23 mg, 0.021 mmol) in methoxycyclopentane (25 mL) for 12 h according to the general procedure for Migita–Kosugi–Stille coupling. The crude product was subjected to column chromatography (silica gel, toluene/hexane, 1:1) and the collected material was subsequently washed with hexane to give **13** (142 mg, 0.30 mmol, 73%) as an orange solid. An analytical sample was obtained by reprecipitation from $CHCl_3$/hexane. M.p. 261–263 °C; ^{1}H NMR (600 MHz, $CDCl_3$): δ = 8.10 (d, *J* = 1.5 Hz, 2H), 8.06 (d, *J* = 8.4 Hz, 2H), 7.96 (d, *J* = 8.4 Hz, 2H), 7.94 (d, *J* = 7.8 Hz, 2H), 7.64–7.58 ppm (m, 2H); ^{13}C NMR (150 MHz, $CDCl_3$): δ = 155.33, 142.91, 133.97, 133.06, 129.49, 129.27, 129.10, 128.76, 128.08, 127.94, 127.91, 127.25, 125.90 ppm; UV/Vis (CH_2Cl_2): λ_{max} (ε) = 310 (10900), 399 nm (6200 $M^{-1}cm^{-1}$); MS (MALDI-TOF, Dith, positive): *m/z*: 479.20 [*M*+H]$^+$; elemental analysis calcd (%) for $C_{26}H_{14}N_4O_4S$·0.03$CHCl_3$: C 64.85, H 2.93, N 11.62; found: C 64.75, H 3.14, N 11.28.

Preparation of 14: Compound **9** (400 mg, 1.04 mmol) was allowed to react with tributyl(2-benzo[*b*]furyl)tin (1.07 g, 2.63 mmol) in the presence of [Pd(PPh$_3$)$_4$] (54 mg, 0.047 mmol) in THF (30 mL) for 28 h according to the general procedure for Migita–Kosugi–Stille coupling. The crude product was subjected to column chromatography (silica gel, toluene/hexane, 1:1) and the collected material was subsequently washed with hexane to give **14** (387 mg, 0.84 mmol, 81%) as a brown solid. An analytical sample was obtained by reprecipitation from $CHCl_3$/hexane. M.p. 266–268 °C; ^{1}H NMR (600 MHz, [D$_6$]DMSO): δ = 8.34 (s, 2H), 7.94 (d, *J* = 7.5 Hz, 2H), 7.68 (d, *J* = 8.1 Hz, 2H), 7.52 (t, *J* = 7.5 Hz, 2H), 7.42 ppm (t, *J* = 8.1 Hz, 2H); ^{13}C NMR (150 MHz, [D$_6$]DMSO): δ = 154.82, 150.06, 144.75, 139.03, 127.84, 127.57, 124.32, 122.94, 115.70, 115.37, 111.51 ppm; UV/Vis (CH_2Cl_2): λ_{max} (ε) = 293 (27200), 445 nm (11400 $M^{-1}cm^{-1}$); MS (MALDI-TOF, DHBA, positive): *m/z*: 458.06 [*M*]$^+$; elemental analysis calcd (%) for $C_{22}H_{10}N_4O_6S$·0.08$CHCl_3$: C 56.67, H 2.17, N 11.97; found: C 56.66, H 2.28, N 11.75.

Preparation of 15: Compound **10** (100 mg, 0.20 mmol) was allowed to react with PPh_3 (543 mg, 2.07 mmol) for 7 h according to the general procedure for PPh_3-mediated reductive cyclization. The crude product was subjected to column chromatography (silica gel; toluene/ethyl acetate, 2:1) and the collected material was subsequently washed with CH_2Cl_2 to give **15** (76 mg, 0.18 mmol, 87%) as an orange solid. M.p. > 300 °C; ^{1}H NMR (600 MHz, [D$_6$]DMSO): δ = 12.67 (s, 2H), 8.22 (d, *J* = 7.9 Hz, 2H), 8.10 (d, *J* = 7.7 Hz, 2H), 7.56 (t, *J* = 7.7 Hz, 2H), 7.42 ppm (t, *J* = 7.9 Hz, 2H); ^{13}C NMR (150 MHz, [D$_6$]DMSO): δ = 147.26, 141.84, 134.88, 129.08, 126.52, 124.93, 124.57, 124.04, 119.94, 117.96, 107.83 ppm; UV/Vis (CH_2Cl_2): λ_{max} (relative intensity) = 273 (0.72), 293 (0.44), 336 (0.81), 353 (1.0), 430 nm (0.25); MS (MALDI-TOF, Dith, positive): *m/z*: 427.12 [*M*+H]$^+$; elemental analysis calcd (%) for $C_{22}H_{10}N_4S_3$: C 61.95, H 2.36, N 13.14; found: C 61.90, H 2.52, N 12.94.

Preparation of 16: Compound **11** (444 mg, 0.90 mmol) was allowed to react with PPh_3 (2.51 g, 9.57 mmol) for 8 h according to the general procedure for PPh_3-mediated reductive cyclization. The crude product was subjected to column chromatography (silica gel; toluene/ethyl acetate, 2:1) and the collected material was further purified by reprecipitation from THF/hexane to give **16** (325 mg, 0.76 mmol, 85%) as an orange solid. M.p. 285–288 °C (decomp.); ^{1}H NMR (600 MHz, [D$_6$]DMSO): δ = 12.52 (s, 2H), 9.10 (d, *J* = 7.6 Hz, 2H), 8.03 (d, *J* = 7.6 Hz, 2H), 7.58 (t, *J* = 7.6 Hz, 2H), 7.38 ppm (t, *J* = 7.6 Hz, 2H); ^{13}C NMR (150 MHz, [D$_6$]DMSO): δ = 147.64, 138.99, 135.97, 131.46, 129.04, 125.01, 124.90, 123.90, 123.83, 123.33, 123.18, 122.28, 122.23, 121.13, 107.17 ppm (two pairs of signals are observed due to slow conformational exchange on the NMR timescale); UV/Vis (CH_2Cl_2): λ_{max} (relative intensity) = 273 (0.71), 293 (0.44), 336 (0.81), 353 (1.0), 430 nm (0.25); MS (MALDI-TOF, Dith, positive): *m/z*: 426.03 [*M*]$^+$; elemental analysis calcd (%) for $C_{22}H_{10}N_4S_3$·0.5THF: C 62.31, H 3.05, N 12.11; found: C 62.31, H 3.73, N 10.95.

Preparation of 17: Compound **12** (92 mg, 0.19 mmol) was allowed to react with PPh_3 (510 mg, 1.94 mmol) for 17 h according to the general procedure for PPh_3-mediated reductive cyclization. The crude product was subjected to column chromatography (silica gel; toluene/ethyl acetate, 3:1) and the collected material was further purified by reprecipitation from $CHCl_3$/hexane to give **17** (69 mg, 0.16 mmol, 87%) as a yellow solid. M.p. > 300 °C; ^{1}H NMR (600 MHz, [D$_6$]DMSO): δ = 12.44 (s, 2H), 10.76 (d, *J* = 8.0 Hz, 2H), 8.11 (d, *J* = 8.0 Hz, 2H), 8.06 (d, *J* = 9.0 Hz, 2H), 7.98 (d, *J* = 9.0 Hz, 2H), 7.82 (t, *J* = 8.0 Hz, 2H), 7.59 ppm (t, *J* = 8.0 Hz, 2H); ^{13}C NMR (150 MHz, [D$_6$]DMSO): δ = 149.13, 135.32, 129.71, 128.66, 128.57, 128.31, 126.56, 126.16, 126.10, 124.03, 118.50, 113.92, 109.31 ppm; UV/Vis (CH_2Cl_2): λ_{max} (ε) = 281 (28700), 296 (29000), 323 (20300), 340 (28500), 355 (39500), 423 nm (13700 $M^{-1}cm^{-1}$); MS (MALDI-TOF, Dith, positive): *m/z*: 415.25 [*M*+H]$^+$; elemental analysis calcd (%) for $C_{26}H_{14}N_4S$ 0.04$CHCl_3$: C 74.60, H 3.37, N 13.36; found: C 74.39, H 3.58, N 13.23.

Preparation of 18: Compound **13** (45 mg, 0.094 mmol) was allowed to react with PPh_3 (251 mg, 0.957 mmol) for 24 h according to the general procedure for PPh_3-mediated reductive cyclization. The crude product was subjected to column chromatography (silica gel; toluene/ethyl acetate, 5:1) and the collected material was subsequently washed with CH_2Cl_2 to give **18** (34 mg, 0.082 mmol, 87%) as an orange solid. M.p. > 300 °C; ^{1}H NMR (600 MHz, [D$_6$]DMSO): δ = 12.55 (s, 2H), 8.57 (d, *J* = 8.4 Hz, 2H), 8.42 (d, *J* = 7.8 Hz, 2H), 8.14 (d, *J* = 7.8 Hz, 2H), 7.88 (d, *J* = 8.4 Hz, 2H), 7.80 (t, *J* = 7.8 Hz, 2H), 7.63 ppm (t, *J* = 7.8 Hz, 2H); ^{13}C NMR (150 MHz, [D$_6$]DMSO): δ = 148.95, 132.73, 130.96, 128.98, 127.83, 126.48, 125.18, 122.19, 121.51, 120.63, 119.88, 119.65, 108.82 ppm; UV/Vis (CH_2Cl_2): λ_{max} (relative intensity) = 282 (0.73), 297 (0.73), 324 (0.51), 340 (0.72), 356 (1.0), 423 nm (0.35); MS (MALDI-TOF, Dith, positive): *m/z*: 415.26 [*M*+H]$^+$; elemental analysis calcd (%) for $C_{26}H_{14}N_4S$: C 75.34, H 3.40, N 13.52; found: C 75.44, H 3.67, N 13.24.

Preparation of 19: Compound **14** (150 mg, 0.33 mmol) was allowed to react with PPh_3 (858 mg, 3.27 mmol) for 9 h according to the general procedure for PPh_3-mediated reductive cyclization. The crude product was subjected to column chromatography (silica gel; toluene/ethyl acetate, 3:1) and the collected material was subsequently washed with CH_2Cl_2 to give **19** (77 mg, 0.19 mmol, 60%) as red needles. M.p. > 300 °C; ^{1}H NMR (400 MHz, [D$_6$]DMSO): δ = 12.17 (s, 2H), 7.97 (d, *J* = 7.6 Hz, 2H), 7.80 (d, *J* = 8.0 Hz, 2H), 7.44–7.36 ppm (m, 4H); ^{13}C NMR (150 MHz, [D$_6$]DMSO): δ = 158.98, 146.13, 144.56, 127.27, 123.61, 123.22, 122.77, 118.41, 118.24, 112.60, 98.39 ppm; UV/Vis (CH_2Cl_2): λ_{max} (relative intensity) = 337 (1.0), 354 (0.99), 438 nm (0.27); HRMS (FAB, NBA, positive): *m/z* calcd for $C_{22}H_{10}N_4O_2S^+$: 394.0524; found 394.0517 [*M*]$^+$.

Preparation of 4: Compound **15** (100 mg, 0.23 mmol) was allowed to react with iodoethane (770 mg, 4.9 mmol) in the presence of

sodium hydride (60% in oil, 293 mg, 7.1 mmol) for 10 h according to the general procedure for *N*-ethylation. The crude product was purified by column chromatography (silica gel; hexane/toluene, 2:1) to give **4** (95 mg, 0.20 mmol, 84%) as an orange solid. An analytical sample was obtained by reprecipitation from $CHCl_3$/hexane. M.p. 279–281 °C; ^{1}H NMR (400 MHz, $CDCl_3$): δ = 8.06 (d, J = 7.6 Hz, 2H), 8.01 (d, J = 7.6 Hz, 2H), 7.53 (t, J = 7.6 Hz, 2H), 7.40 (t, J = 7.6 Hz, 2H), 5.00 (q, J = 7.2 Hz, 4H), 1.25 ppm (t, J = 7.2 Hz, 6H); ^{13}C NMR (150 MHz, $CDCl_3$): δ = 148.16, 143.70, 138.25, 132.93, 127.57, 124.98, 124.91, 123.86, 122.71, 119.68, 112.32, 45.75, 15.48 ppm; UV/Vis (CH_2Cl_2): λ_{max} (ε) = 277 (30600), 293 (18900), 341 (34000) 357 (40500), 443 nm (11800 $M^{-1}cm^{-1}$); MS (MALDI-TOF, Dith, positive): *m/z*: 483.23 $[M+H]^+$; elemental analysis calcd (%) for $C_{26}H_{18}N_4S_3$·0.025$CHCl_3$: C 64.36, H 3.74, N 11.54; found: C 64.21, H 3.89, N 11.44.

Preparation of 5: Compound **16** (50 mg, 0.12 mmol) was allowed to react with iodoethane (151 mg, 0.97 mmol) in the presence of sodium hydride (60% in oil, 61 mg, 1.53 mmol) for 4 days according to the general procedure for *N*-ethylation. The precipitate formed was collected by filtration and purified by column chromatography (silica gel; toluene) to give **5** (4 mg, 8.3 μmol, 8%) as a red solid. An analytical sample was obtained by reprecipitation from $CHCl_3$/hexane. M.p. > 300 °C; ^{1}H NMR (400 MHz, $CDCl_3$): δ = 9.39 (d, J = 7.7 Hz, 2H), 7.88 (d, J = 7.7 Hz, 2H), 7.62 (t, J = 7.7 Hz, 2H), 7.39 (t, J = 7.7 Hz, 2H), 4.55 (q, J = 7.2 Hz, 4H), 1.66 ppm (t, J = 7.2 Hz, 6H); ^{13}C NMR: not available due to poor solubility; UV/Vis (CH_2Cl_2): λ_{max} (relative intensity) = 264 (1.0), 295 (0.60), 363 (0.21), 452 nm (0.16); HRMS (FAB, NBA, positive): *m/z* calcd for $C_{26}H_{18}N_4S_3^+$: 482.0694; found: 482.0688 $[M]^+$.

Preparation of 6: Compound **17** (30 mg, 0.072 mmol) was allowed to react with iodoethane (78 mg, 0.50 mmol) in the presence of sodium hydride (60% in oil, 100 mg, 2.48 mmol) for 26 h according to the general procedure for *N*-ethylation. The crude product was purified by column chromatography (silica gel; hexane/toluene, 1:4) to give **6** (28 mg, 0.060 mmol, 82%) as an orange solid. An analytical sample was obtained by reprecipitation from $CHCl_3$/hexane. M.p. 298–300 °C; ^{1}H NMR (600 MHz, $CDCl_3$): δ = 10.92 (d, J = 9.0 Hz, 2H), 8.06 (d, J = 7.8 Hz, 2H), 7.98 (d, J = 9.0 Hz, 2H), 7.89–7.85 (m, 4H), 7.63 (ddd, J = 7.8, 6.6, 1.2 Hz, 2H), 4.92 (q, J = 7.2 Hz, 4H), 1.04 ppm (t, J = 7.2 Hz, 6H); ^{13}C NMR (150 MHz, $CDCl_3$): δ = 149.92, 139.53, 131.86, 130.56, 129.44, 128.64, 127.84, 126.98, 126.66, 124.80, 122.35, 114.87, 112.83, 43.83, 14.32 ppm; UV/Vis (CH_2Cl_2): λ_{max} (ε) = 277 (30900), 303 (32300), 343 (29300) 373 (17600), 434 nm (16100 $M^{-1}cm^{-1}$); MS (MALDI-TOF, Dith, positive): *m/z*: 471.32 $[M+H]^+$; elemental analysis calcd (%) for $C_{30}H_{22}N_4S$·0.02$CHCl_3$: C 76.23, H 4.69, N 11.84; found: C 76.26, H 4.78, N 11.79.

Preparation of 7: Compound **18** (19 mg, 0.046 mmol) was allowed to react with iodoethane (59 mg, 0.37 mmol) in the presence of sodium hydride (60% in oil, 36 mg, 0.92 mmol) for 24 h according to the general procedure for *N*-ethylation. The crude product was purified by column chromatography (silica gel; hexane/toluene, 4:1) to give **7** (13 mg, 0.028 mmol, 62%) as a yellow solid. An analytical sample was obtained by reprecipitation from $CHCl_3$/hexane. M.p. 290–293 °C; ^{1}H NMR (600 MHz, $CDCl_3$): δ = 8.90 (d, J = 8.4 Hz, 2H), 8.58 (d, J = 8.3 Hz, 2H), 8.11 (d, J = 8.0 Hz, 2H), 7.95 (d, J = 8.4 Hz, 2H), 7.72 (ddd, J = 8.3, 6.8, 1.2 Hz, 2H), 7.59 (ddd, J = 8.0, 6.8, 1.2 Hz, 2H), 5.29 (q, J = 7.2 Hz, 4H), 0.91 ppm (t, J = 7.2 Hz, 6H); ^{13}C NMR (150 MHz, $CDCl_3$): δ = 149.90, 136.79, 133.91, 132.66, 129.94, 126.30, 125.23, 124.89, 124.71, 123.88, 121.82, 120.92, 113.94, 47.14, 14.01 ppm; UV/Vis (CH_2Cl_2): λ_{max} (ε) = 252 (27900), 291 (69800), 326 (31200) 339 (36900), 362 (12100), 383 (18700), 429 nm (15500 $M^{-1}cm^{-1}$); MS (MALDI-TOF, Dith, positive): *m/z*: 471.26 $[M+H]^+$; elemental analysis calcd (%) for $C_{30}H_{22}N_4S$·0.17$CHCl_3$: C 73.82, H 4.55, N 11.41; found: C 73.74, H 4.76, N 11.37.

Preparation of 8: Compound **19** (35 mg, 0.089 mmol) was allowed to react with iodoethane (307 mg, 1.97 mmol) in the presence of sodium hydride (60% in oil, 109 mg, 2.74 mmol) for 48 h according to the general procedure for *N*-ethylation. The crude product was purified by column chromatography (silica gel; toluene) to give **8** (12 mg, 0.027 mol, 30%) as a red solid. An analytical sample was obtained by reprecipitation from CH_2Cl_2/hexane. M.p. > 300 °C; ^{1}H NMR (400 MHz, $CDCl_3$): δ = 7.79–7.75 (m, 4H), 7.41–7.35 (m, 4H), 4.75 (q, J = 7.2 Hz, 4H), 1.54 ppm (t, J = 7.2 Hz, 6H); ^{13}C NMR (150 MHz, $CDCl_3$): δ = 160.05, 146.84, 146.67, 130.66, 123.96, 123.42, 117.42, 113.47, 103.23, 45.79, 15.85 ppm (two signals are missing); UV/Vis (CH_2Cl_2): λ_{max} (ε) = 257 (27700), 288 (13800), 312 (22100), 342 (56900), 360 (66900), 451 nm (15200 $M^{-1}cm^{-1}$); MS (MALDI-TOF, Dith, positive): *m/z*: 450.15 $[M]^+$; elemental analysis calcd (%) for $C_{26}H_{18}N_4O_2S$·0.12CH_2Cl_2: C 68.10, H 3.99, N 12.16; found: C 68.01, H 4.05, N 12.11.

Acknowledgements

This work was financially supported by Grants-in-Aid for Young Scientists from MEXT, Japan, and a research grant from the Kurata Memorial Hitachi Science and Technology Foundation. This work was performed under the Cooperative Research Program of "Network Joint Research Center for Materials and Devices" (Osaka University and Kyushu University). The authors thank Mr. Taisuke Matsumoto (Kyushu University) for helpful assistance in X-ray diffraction analyses, Ms. Yasuko Tokitoh (Kyushu University) for helpful assistance in mass spectroscopic analyses, and Prof. Soichiro Kyushin (Gunma University) for generous permission to use the X-ray diffractometer.

Keywords: electrochemistry · fluorescence · fused-ring systems · polymorphism · X-ray diffraction

[1] a) A. C. Grimsdale, K. Müllen, *Macromol. Rapid Commun.* **2007**, *28*, 1676; b) I. F. Perepichka, D. F. Perepichka, *Handbook of Thiophene-Based Materials*, Wiley-VCH, Weinheim, **2009**; c) P. M. Beaujuge, J. M. J. Fréchet, *J. Am. Chem. Soc.* **2011**, *133*, 20009; d) H. Usta, A. Facchetti, T. J. Marks, *Acc. Chem. Res.* **2011**, *44*, 501; e) L. Chen, Y. Hernandez, X. Feng, K. Müllen, *Angew. Chem. Int. Ed.* **2012**, *51*, 7640; *Angew. Chem.* **2012**, *124*, 7758; f) C. Wang, H. Dong, W. Hu, Y. Liu, D. Zhu, *Chem. Rev.* **2012**, *112*, 2208.

[2] a) J. E. Anthony, *Angew. Chem. Int. Ed.* **2008**, *47*, 452; *Angew. Chem.* **2008**, *120*, 460; b) Z. Sun, Q. Ye, C. Chi, J. Wu, *Chem. Soc. Rev.* **2012**, *41*, 7857.

[3] For example: a) C. D. Simpson, J. D. Brand, A. J. Berresheim, L. Przybilla, H. J. Räder, K. Müllen, *Chem. Eur. J.* **2002**, *8*, 1424; b) M. M. Payne, S. R. Parkin, J. E. Anthony, *J. Am. Chem. Soc.* **2005**, *127*, 8028; c) D. Chun, Y. Cheng, F. Wudl, *Angew. Chem. Int. Ed.* **2008**, *47*, 8380; *Angew. Chem.* **2008**, *120*, 8508; d) Y. Li, L. Xu, T. Liu, Y. Yu, H. Liu, Y. Li, D. Zhu, *Org. Lett.* **2011**, *13*, 5692; e) B. Purushothaman, M. Bruzek, S. R. Parkin, A.-F. Miller, J. E. Anthony, *Angew. Chem. Int. Ed.* **2011**, *50*, 7013; *Angew. Chem.* **2011**, *123*, 7151; f) M. Watanabe, Y. J. Chang, S.-W. Liu, T.-H. Chao, K. Goto, Md. M. Islam, C.-H. Yuan, Y.-T. Tao, T. Shinmyozu, T. J. Chow, *Nat. Chem.* **2012**, *4*, 574; g) J. Xiao, H. M. Duong, Y. Liu, W. Shi, L. Ji, G. Li, S. Li, X.-W. Liu, J. Ma, F. Wudl, Q. Zhang, *Angew. Chem. Int. Ed.* **2012**, *51*, 6094; *Angew. Chem.* **2012**, *124*, 6198.

[4] a) K. Takimiya, S. Shimamura, I. Osaka, E. Miyazaki, *Adv. Mater.* **2011**, *23*, 4347; b) K. Takimiya, M. Nakano, M. J. Kang, E. Miyazaki, I. Osaka, *Eur. J. Org. Chem.* **2013**, 217; c) U. H. F. Bunz, *Chem. Eur. J.* **2009**, *15*, 6780;

d) U. H. F. Bunz, J. U. Engelhart, B. D. Lindner, M. Schaffroth, *Angew. Chem. Int. Ed.* **2013**, *52*, 3810; *Angew. Chem.* **2013**, *125*, 3898; e) Q. Miao, *Synlett* **2012**, *23*, 326; f) Q. Miao, *Adv. Mater.* **2014**, *26*, 5541; g) T. Baumgartner, *Acc. Chem. Res.* **2014**, *47*, 1613.

[5] A. Fukazawa, S. Yamaguchi, *Chem. Asian J.* **2009**, *4*, 1386.

[6] a) R. Gompper, H. U. Wagner, *Angew. Chem. Int. Ed. Engl.* **1988**, *27*, 1437; *Angew. Chem.* **1988**, *100*, 1492; b) M. Barzoukas, M. Blanchard-Desce in *Adv. Multi-Photon Processes. Spectrosc., Vol. 13* (Eds.: S. H. Lin, A. A. Villaeys, Y. Fujimura) World Scientific, Singapore, **2001**, p. 261; c) H. Meier, *Angew. Chem. Int. Ed.* **2005**, *44*, 2482; *Angew. Chem.* **2005**, *117*, 2536.

[7] a) S. Barlow, S. R. Marder in *Functional Organic Materials* (Eds.: T. J. J. Müller, U. H. F. Bunz), Wiley-VCH, Weinheim, **2007**, p. 393; b) M. Kivala, F. Diederich, *Acc. Chem. Res.* **2009**, *42*, 235; c) S.-i. Kato, F. Diederich, *Chem. Commun.* **2010**, *46*, 1994; d) A. J. Zucchero, P. L. Mcgrier, U. H. F. Bunz, *Acc. Chem. Res.* **2010**, *43*, 397; e) A. Mishra, P. Bäuerle, *Angew. Chem. Int. Ed.* **2012**, *51*, 2020; *Angew. Chem.* **2012**, *124*, 2060; f) J. E. Coughlin, Z. B. Henson, G. C. Welch, G. C. Bazan, *Acc. Chem. Res.* **2014**, *47*, 257.

[8] a) X. Zhang, X. Zhang, W. Shi, X. Meng, C.-S. Lee, S.-T. Lee, *Angew. Chem. Int. Ed.* **2007**, *46*, 1525; *Angew. Chem.* **2007**, *119*, 1547; b) X. Zhang, X. Zhang, K. Zou, C.-S. Lee, S.-T. Lee, *J. Am. Chem. Soc.* **2007**, *129*, 3527.

[9] a) J. Xu, L. Wen, W. Zhou, J. Lv, Y. Guo, M. Zhu, H. Liu, Y. Li, L. Jiang, *J. Phys. Chem. C* **2009**, *113*, 5924; b) J. Xu, H. Zheng, H. Liu, C. Zhou, Y. Zhao, Y. Li, Y. Li, *J. Phys. Chem. C* **2010**, *114*, 2925; c) S. Chen, Y. Li, C. Liu, W. Yang, Y. Li, *Eur. J. Org. Chem.* **2011**, 6445; see also reviews: d) H. Liu, J. Xu, Y. Li, Y. Li, *Acc. Chem. Res.* **2010**, *43*, 1496; e) Y. Li, T. Liu, H. Liu, M.-Z. Tian, Y. Li, *Acc. Chem. Res.* **2014**, *47*, 1186.

[10] S.-i. Kato, T. Furuya, A. Kobayashi, M. Nitani, Y. Ie, Y. Aso, T. Yoshihara, S. Tobita, Y. Nakamura, *J. Org. Chem.* **2012**, *77*, 7595.

[11] A few thiadiazole derivatives with electron-donating heteroaromatics have been sporadically reported, see: a) L. Biniek, I. Bulut, P. Lévêque, T. Heiser, N. Leclerc, *Tetrahedron Lett.* **2011**, *52*, 1811; b) Y.-S. Cheng, C.-H. Chen, Y.-J. Ho, S.-W. Chang, H. A. Witek, C.-S. Hsu, *Org. Lett.* **2011**, *13*, 5484.

[12] a) X. Naraso, J.-i. Nishida, S. Ando, J. Yamaguchi, K. Itaka, H. Koinuma, H. Tada, S. Tokito, Y. Yamashita, *J. Am. Chem. Soc.* **2005**, *127*, 10142; b) X. Naraso, J.-i. Nishida, D. Kumaki, S. Tokito, Y. Yamashita, *J. Am. Chem. Soc.* **2006**, *128*, 9598.

[13] a) C.-Y. Jia, S.-X. Liu, C. Tanner, C. Leiggener, L. Sanguinet, E. Levillain, S. Leutwyler, A. Hauser, S. Decurtins, *Chem. Commun.* **2006**, 1878; b) X. Guégano, A. L. Kanibolotsky, C. Blum, S. F. L. Mertens, S.-X. Liu, A. Neels, H. Hagemann, P. J. Skabara, S. Leutwyler, T. Wandlowski, A. Hauser, S. Decurtins, *Chem. Eur. J.* **2009**, *15*, 63; c) M. Jaggi, C. Blum, B. S. Marti, S.-X. Liu, S. Leutwyler, S. Decurtins, *Org. Lett.* **2010**, *12*, 1344; d) H.-P. Jia, J. Ding, Y.-F. Ran, S.-X. Liu, C. Blum, I. Petkova, A. Hauser, S. Decurtins, *Chem. Asian J.* **2011**, *6*, 3312; e) H. Jia, J. Ding, A. Hauser, S. Decurtins, S.-X. Liu, *Asian J. Org. Chem.* **2014**, *3*, 198.

[14] Y. Yang, Y. Wang, Y. Xie, T. Xiong, Z. Yuan, Y. Zhang, S. Qian, Y. Xiao, *Chem. Commun.* **2011**, *47*, 10749.

[15] C. Seillan, H. Brisset, O. Siri, *Org. Lett.* **2008**, *10*, 4013.

[16] Q. Tang, J. Liu, H. S. Chan, Q. Miao, *Chem. Eur. J.* **2009**, *15*, 3965.

[17] In the previous work,[10] the synthesis of furopyrrole-fused thiadiazole derivatives were unsuccessful.

[18] A. P. Zoombelt, M. Fonrodona, M. G. R. Turbiez, M. M. Wienk, R. A. J. Janssen, *J. Mater. Chem.* **2009**, *19*, 5336.

[19] a) J. I. G. Cadogan, *Organophosphorous Reagents in Organic Synthesis*, Academic Press, London, **1979**; Chapter 6; b) A. W. Freeman, M. Urvoy, M. E. Criswell, *J. Org. Chem.* **2005**, *70*, 5014.

[20] The Stille coupling reaction with tributyl(3-benzo[*b*]furyl)tin has been reported: H. Nakamura, M. Aizawa, D. Takeuchi, A. Murai, O. Shimomura, *Tetrahedron Lett.* **2000**, *41*, 2185.

[21] Gaussian 09, Revision B.01, M. J. Frisch, G. W. Trucks, H. B. Schlegel, G. E. Scuseria, M. A. Robb, J. R. Cheeseman, G. Scalmani, V. Barone, B. Mennucci, G. A. Petersson, H. Nakatsuji, M. Caricato, X. Li, H. P. Hratchian, A. F. Izmaylov, J. Bloino, G. Zheng, J. L. Sonnenberg, M. Hada, M. Ehara, K. Toyota, R. Fukuda, J. Hasegawa, M. Ishida, T. Nakajima, Y. Honda, O. Kitao, H. Nakai, T. Vreven, J. A. Montgomery, Jr., J. E. Peralta, F. Ogliaro, M. Bearpark, J. J. Heyd, E. Brothers, K. N. Kudin, V. N. Staroverov, R. Kobayashi, J. Normand, K. Raghavachari, A. Rendell, J. C. Burant, S. S. Iyengar, J. Tomasi, M. Cossi, N. Rega, J. M. Millam, M. Klene, J. E. Knox, J. B. Cross, V. Bakken, C. Adamo, J. Jaramillo, R. Gomperts, R. E. Stratmann, O. Yazyev, A. J. Austin, R. Cammi, C. Pomelli, J. W. Ochterski, R. L. Martin, K. Morokuma, V. G. Zakrzewski, G. A. Voth, P. Salvador, J. J. Dannenberg, S. Dapprich, A. D. Daniels, Ö. Farkas, J. B. Foresman, J. V. Ortiz, J. Cioslowski, D. J. Fox, Gaussian, Inc., Wallingford CT, **2009**.

[22] The close proximity between the naphthalene and thiadiazole moieties in **6** demonstrated by X-ray crystallographic analyses hints at intramolecular through-space interactions, which may also bring about the differences in the properties of **6** and **7**.

[23] The $E_T(30)$ parameters (33.9 kcal mol^{-1} for toluene, 37.4 kcal mol^{-1} for THF, 38.1 kcal mol^{-1} for EtOAc, 40.7 kcal mol^{-1} for CH_2Cl_2, 42.9 kcal mol^{-} for DMF) are taken from: C. Reichardt, *Chem. Rev.* **1994**, *94*, 2319.

[24] For details of experimental methods, see: A. Kobayashi, K. Takehira, T. Yoshihara, S. Uchiyama, S. Tobita, *Photochem. Photobiol. Sci.* **2012**, *11*, 1368.

[25] Preliminary p-type OFET performances of **4** and **8** are summarized in Figure S23 in the Supporting Information.

[26] For a discussion on the HOMO and LUMO levels of **1**–**8** based on DFT calculations, see the Supporting Information.

[27] a) M. Shimizu, T. Hiyama, *Chem. Asian J.* **2010**, *5*, 1516; b) S. S. Babu, K. K. Kartha, A. Ajayaghosh, *J. Phys. Chem. Lett.* **2010**, *1*, 3413; c) Y. Hong, J. W. Y. Lam, B. Z. Tang, *Chem. Soc. Rev.* **2011**, *40*, 5361.

[28] J. B. Birks, *Photophysics of Aromatic Molecules*, Wiley, London, **1970**.

[29] Single crystals of **5** were not obtained despite numerous attempts; the severe insolubility of **5** resulted in its precipitation as a powder.

[30] The crystals **4-Crys.**(**O**) and **4-Crys.**(**G**) are classified as pseudopolymorphs to be exact, because solvent molecules are included in the latter.

[31] In **8-Crys.**, $CHCl_3$ molecules from the solvent of recrystallization are included in a stoichiometry of 1:2.

[32] The space between the neighboring columns is occupied by toluene molecules, which serve as an adhesive (see Figure S1 in the Supporting Information).

[33] H. Shigemitsu, I. Hisaki, E. Kometani, D. Yasumiya, Y. Sakamoto, K. Osaka, T. S. Thakur, A. Saeki, S. Seki, F. Kimura, T. Kimura, N. Tohnai, M. Miyata, *Chem. Eur. J.* **2013**, *19*, 15366.

[34] CH–π and CH–S interactions are observed between **4** and toluene molecules in the packing of **4-Crys.**(**G**), and no π–π stacking interactions are observable.

[35] The crystalline samples were carefully used.

[36] Thoroughly ground crystals of **1**–**4** and **6**–**8** as powder samples were also confirmed to be microcrystals by X-ray diffraction (XRD) measurements (see Figure S7 in the Supporting Information).

[37] In the crystal structure of **7**, S–π interactions instead of π–π stacking interactions are observed.

[38] We performed single-point calculations on **4**·toluene complexes based on the X-ray crystal structure of **4-Crys.**(**G**), and the results suggest that the proximity of the toluene molecule to the sulfur atom of **4** tends to decrease the HOMO–LUMO gaps (see Figure S21 in the Supporting Information).

[39] According to the DFT calculations at the B3LYP/6-311G** level of theory, the $\Delta E_{H\text{-}L}$ values of the monomers in **1-Crys.**(**Y**), **2-Crys.**(**O**), **4-Crys.**(**O**), and **6-Crys.**(**O**) are comparable to those in **1-Crys.**(**G**), **2-Crys.**(**G**), **4-Crys.**(**G**), and **6-Crys.**(**G**), respectively. The differences in the $\Delta E_{H\text{-}L}$ values is at most 0.03 eV (see Table S4 in the Supporting Information), which may reflect differences in the planarity of the monomers.

[40] We also estimated the intermolecular transfer integrals (*t*) of the HOMOs and LUMOs in the dimers formed in the crystals of **1**–**4**, **6**, and **8** at the PW91/TZP level of theory with the Amsterdam density functional (ADF) program (ADF2010.01, SCM (Scientific Computing and Modeling), Theoretical Chemistry, Vrije Universiteit, Amsterdam, The Netherlands, **2010**, http://www.scm.com. The relationship between the *t* values and the degree of electronic interactions in the dimers is discussed in the Supporting Information (see Table S5).

[41] V. Coropceanu, J. Cornil, D. A. da Silva Filho, Y. Olivier, R. Silbey, J.-L. Brédas, *Chem. Rev.* **2007**, *107*, 926.

[42] a) F. C. Spano, *Acc. Chem. Res.* **2010**, *43*, 429; b) J. Gierschner, Y.-S. Huang, B. Van Averbeke, J. Cornil, R. H. Friend, D. Beljonne, *J. Chem. Phys.* **2009**, *130*, 044105; c) J. Gierschner, S. Y. Park, *J. Mater. Chem. C* **2013**, *1*, 5818.

[43] a) E. G. McRae, M. Kasha, *J. Chem. Phys.* **1958**, *28*, 721; b) M. Kasha, R. Rawls, M. A. El-Bayoumi, *Pure Appl. Chem.* **1965**, *11*, 371.

[44] F. Würthner, T. E. Kaiser, C. R. Saha-Möller, *Angew. Chem. Int. Ed.* **2011**, *50*, 3376; *Angew. Chem.* **2011**, *123*, 3436, and references therein.
[45] We carried out single-point calculations on **8**·$CHCl_3$ complexes based on the X-ray crystal structure, and the results suggest that the close proximity of the $CHCl_3$ molecule to the benzene rings of **8** tends to decrease the HOMO–LUMO gaps (see Figure S22 in the Supporting Information). The favorable interaction of benzene with $CHCl_3$ is demonstrated by high-level ab initio calculations: S. Tsuzuki, K. Honda, T. Uchimaru, M. Mikami, K. Tanabe, *J. Phys. Chem. A* **2002**, *106*, 4423.
[46] It has been pointed out by Zhang, Wang, and co-workers that the packing along one distinct direction usually consists of a component of *J*-aggregation and a component of *H*-aggregation: T. Zhou, F. Li, Y. Fan, W. Song, X. Mu, H. Zhang, Y. Wang, *Chem. Commun.* **2009**, 3199. Hence, it is likely that the ratio of the components of *J*- and *H*-aggregation is sensitive to the nature of the molecule, the area of overlap of the adjacent molecules, and the intermolecular separation.

Received: October 1, 2014
Published online on ■■ ▮▮, 0000

FULL PAPER

π-Extended thiadiazoles: The photophysical and electrochemical properties of a series of π-extended thiadiazoles fused with electron-donating heteroaromatic moieties are disclosed. These compounds form poly- and pseudopolymorphic crystals, and the fluorescence properties in the crystalline state are significantly affected by the molecular arrangement (see figure).

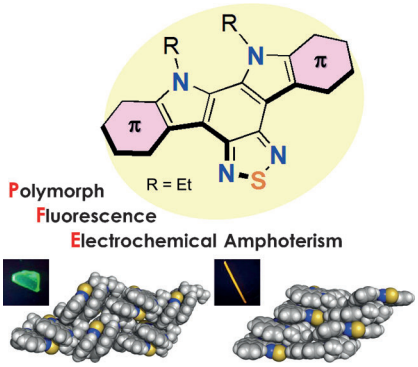

Donor–Acceptor Systems

*S.-i. Kato, T. Furuya, M. Nitani, N. Hasebe, Y. Ie, Y. Aso, T. Yoshihara, S. Tobita, Y. Nakamura**

■■ – ■■

A Series of π-Extended Thiadiazoles Fused with Electron-Donating Heteroaromatic Moieties: Synthesis, Properties, and Polymorphic Crystals